A Strain Tensor Method

for

Three-Dimensional Optimal Michell Structures

by

Benjamin Jacot

Diplôme d'Ingénieur,
École Nationale des Ponts et Chaussées (2015)

Submitted to the Department of Civil and Environmental Engineering
in partial fulfillment of the requirements for the degree of

Master of Engineering

at the

MASSACHUSETTS INSTITUTE OF TECHNOLOGY

June 2016

Author . . . .
Department of Civil and Environmental Engineering
May 18, 2016

Certified by . . . .
Caitlin T. Mueller
Assistant Professor of Architecture and Civil & Environmental
Engineering
Thesis Supervisor

Accepted by . . . .
Heidi Nepf
Chairman, Department Committee on Graduate Theses

A Strain Tensor Method

for

Three-Dimensional Optimal Michell Structures

by

Benjamin Jacot

Submitted to the Department of Civil and Environmental Engineering
on May 18, 2016, in partial fulfillment of the
requirements for the degree of
Master of Engineering

Abstract

In the design of discrete structures such as trusses and frames, important quantitative goals such as minimal weight or minimal compliance often dominate. Many numerical techniques exist to address these needs. However, an analytical approach exists to meet similar goals, which was initiated by A.G.M. Michell (1904) and has been mostly used for two-dimensional structures so far.

This thesis develops a method to extend the existing mainly two-dimensional approach to apply to three-dimensional structures. It will be referred as the Michell strain tensor method (MSTM). First, the proof that MSTM is consistent with the existing theory in two dimensions is provided. Second, two-dimensional known solutions will be replicated based on MSTM. Finally, MSTM will be used to solve new three-dimensional cases.

Thesis Supervisor: Caitlin T. Mueller
Title: Assistant Professor of Architecture and Civil & Environmental Engineering

Acknowledgments

My first thanks go to my thesis advisor Professor Caitlin Mueller, whose communicative passion and wide knowledge on Structural Optimization have helped me moving forward in every steps of this research thesis. I am also grateful to her for letting me chose my thesis topic.

I also thank Alessandro Beghini and Bill Baker from Skidmore, Owings and Merrill, for introducing Michell theory to me for the first time during my internship at SOM San Francisco and for kindly sharing their impressive knowledge of the topic. Along with my Academic Director at École Nationale des Ponts et Chaussées, Romain Mège, they supported my application to MIT. I am grateful to the three of them for this.

A special thank also to David Foxe for showing me Professor Zalewski's work on conceiving buildings inspired by Michell structures.

I finally thank all my schoolmates and friends from MIT for making this year an exceptional experience, my lifelong friends Cécile, Jérémy and Paul for being present despite the distance, and my grandparents, parents and sisters for their unconditional support and trust.

THIS PAGE INTENTIONALLY LEFT BLANK

Contents

THIS PAGE INTENTIONALLY LEFT BLANK

List of Figures

Chapter 1

Introduction

This thesis presents new work in the analytical design of optimum structures, expanding on the pioneering work of A.G.M. Michell in 1904 [1]. This chapter introduces the topic and motivates the need for highly efficient three-dimensional structures, and discusses key applications of such structures.

1.1 Motivation

1.1.1 Designing lightweight structures

Environmental impact of lightweight structures

Lightweight structures are by definition structures that require minimal amounts of material to resist given loading conditions. As a consequence, a lightweight structure takes minimal environmental costs for its constitutive elements to be produced. Metrics already exist to estimate such environmental costs, such as the embodied carbon metric (EC) in Vukotic et al.[2], which is the quantity of emitted CO_2 by unit of quantity of produced material. According to De Wolf[3], an analysis of the ICE, Athena, GaBi and EcoInvent databases indicates that the EC for concrete is 0.15 $kg_{CO_2}/kg_{concrete}$, and 1.2 kg_{CO_2}/kg_{steel} for steel. The aim of conceiving a lightweight

structure is therefore to minimize the material weights by which such factors are multiplied. Lightweight structures are hence a way for structural engineers to tackle the environmental challenges of our times.

Additionally, a component of the total cost of the structure relates to its material usage, so a lightweight structural design is also able to contribute to cost reduction.

New geometries for structural engineering

Lightweight structures are beautiful problems for structural engineering. They are indeed challenging to design and move the discipline of structural engineering out of its "comfort zone". Typical structures are rarely lightweight; scholars often demonstrate lighter or more efficient solutions to typical problems.

In 2013 for example, unconventional two-dimensional roof structure were found in Beghini et al.[4] by defining and varying the degrees of freedom of the force diagram of one typical roof structure - the force diagram being a graphical representation of the internal static equilibrium of a structure. Such structures turned out to be up to 45% lighter than the initial roof structure, hence proving that typical structural engineering approaches needed to be implemented with new technologies to become lighter structures. Figure 1-1, taken from Beghini et al. [4], shows the details of the aforementioned comparison.

Recent tools have even been developed to show how much heavier or lighter a structure is in comparison with another for identical loading conditions, such as structureFIT[5], developed by Mueller & Ochsendorf[6] in 2013. This computational tool is an excellent way to persuade oneself that many typical solutions are not the lightest structures possible. Starting from the well-known Pratt truss structure for example, undergoing a vertical loading on each of its top nodes, structureFIT is able to generate lighter structures, as shown in figure 1-2. In this figure, scores below each structure correspond to the fraction of volume of the Pratt structure that is required for equilibrium with the loading conditions to be maintained.
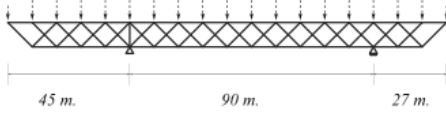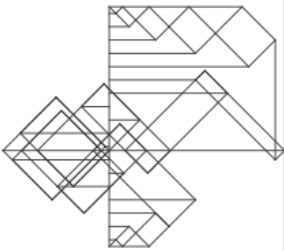
Description	Form Diagram	Force Diagram	Normalized Volume
(a) Initial truss connectivity			1.000
(b) Benchmark truss; top chord, cantilevers and web members unconstrained			0.552

Figure 1-1: Optimization of a roof structure, taken from Beghini et al.[4].
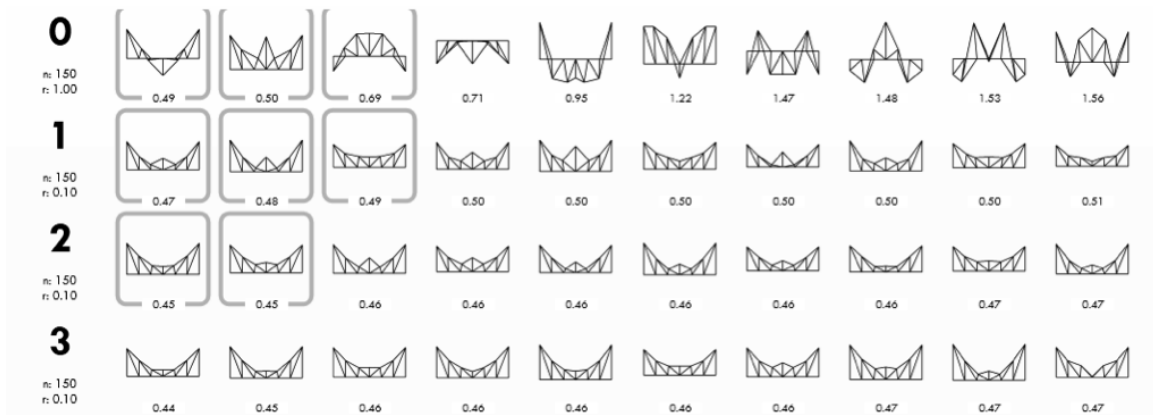
Figure 1-2: Generation of lighter structures through structureFIT[5].

1.1.2 Michell structures: the lightest possible structures

In 1904, Michell[1] initiated a mathematical theory to find the lightest structure possible for a given load case, in two dimensions. This theory will be reviewed in details in section 2.2 *Michell's theorems*. When a solution is found for a given load case and support conditions, the Michell structure is the lightest possible structure, and its volume is an absolute minimum[1]. Michell structures are generated with no

---

[1]See section 2.3.2 *Enhancing Michell's rule for non-equal maximal tension and compression stresses* for discussion about this statement.

constraints on the structure: the latter can have as many tension and compression members as necessary, and its geometry is free to vary anywhere within a predefined planar domain Ω - which often turns out to be the entire plane itself.

Michell structures are purely theoretical: each time, they have an infinite amount of members, each being straight on an infinitesimal length only. However, because they are of absolute minimal volume, they are an excellent source of inspiration for structural engineering. Michell structures indeed give valuable geometrical information that a real structure shall approximate the best way possible so as to be close to optimality in terms of economy of materials.

Existing two-dimensional Michell structures are shown in figures 4-3 and 4-6. The only three-dimensional Michell structure known so far is also shown in figure 5-8 of this thesis. Other Michell structures are shown in figure 1-3, with the location of loads and reactions specified.

1.1.3 Inspiring architects, engineers and designers

Previous sections have shown that general lightweight structures, and Michell structures especially, display original geometries, which perhaps looked counter-intuitive at first sight. They are a source of astonishment, interest or even inspiration for whoever looks at them for the first time, but in any case they turn out to perform better than typical solutions in terms of economy of material.

A motivation for research about Michell structures is then to generate new meaningful structures. They can be used as patterns on which the design of structures can rely.

1.2 Applications of 3D Michell structures

Citing Hemp[7], page 73, "Michell layouts in three-dimensions have a very special character. They have been little studied however." Still, they are of great interest for many applications on which this section will focus.
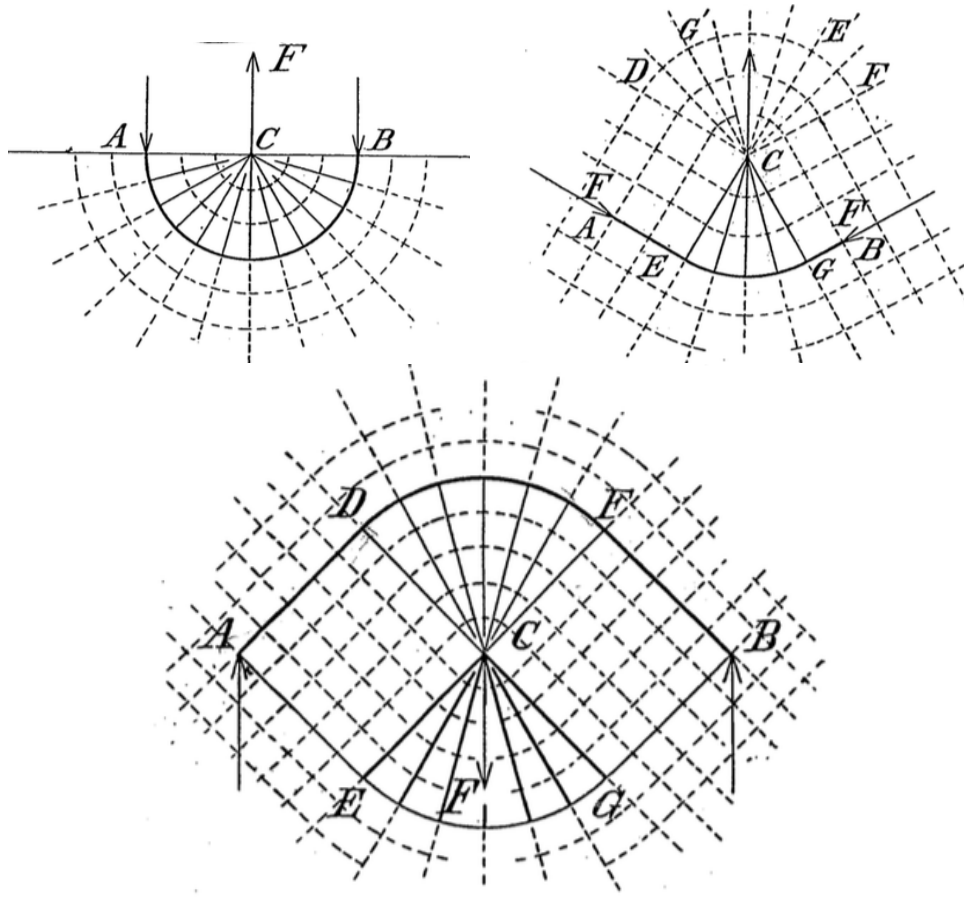
Figure 1-3: Example of Michell structures, taken from Michell[1].

1.2.1 Lateral systems for high-rise buildings

The lateral system of a high-rise building experiences a "premium for height", as shown in Stafford-Smith et al.[8] and reproduced in figure 1-4. What this means is that the quantity of necessary material tends to increase exponentially with height, due to the ever-increasing lateral loads the structure needs to resist. The lateral structure of a high-rise building is hence a direct application for Michell structures and can potentially lead to important economies of material. Because of the scale of such a structure, even a saving of a few percent is not negligible.

The idea of using Michell structures in lateral systems for high-rise buildings has already been implemented [9][10]. This implementation has however always been performed with two-dimensional structures, whereas lateral systems sometimes find their
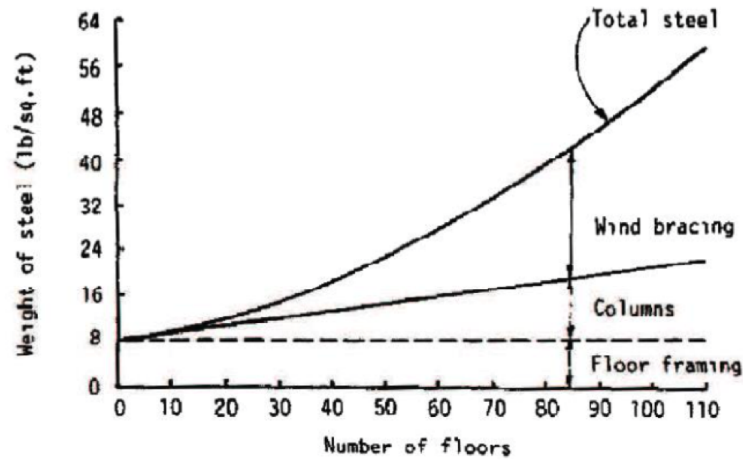
Figure 1-4: The premium for height, as shown in Stafford-Smith et al.[8].

efficiency through three-dimensional design, such as the tube-in-tube system. Therefore, three-dimensional Michell structures may help high-rise buildings to achieve greater economies.

Figure 1-5 shows a SOM competition project for the Transbay Tower competition design for San Francisco inspired by Michell cantilever[10] in 2007. Figure 1-6 shows theoretical buildings inspired by two-dimensional Michell structures imagined by Zalewski[9] in 2005.
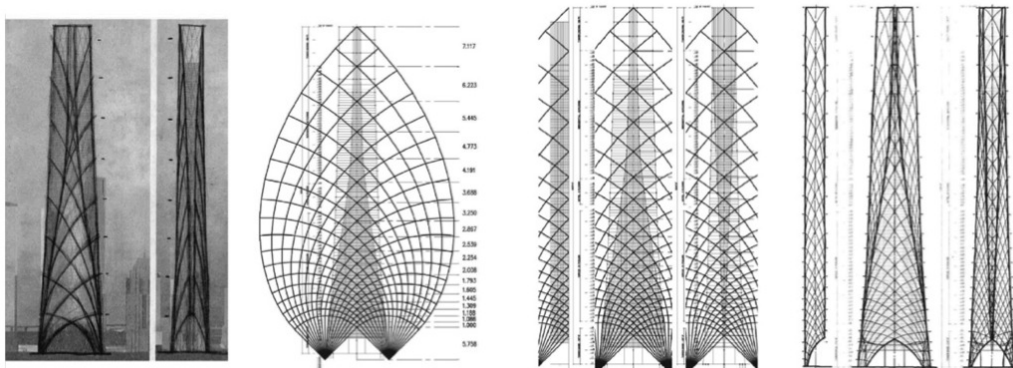
Figure 1-5: A SOM competition project inspired by 2D Michell structures, from [10].
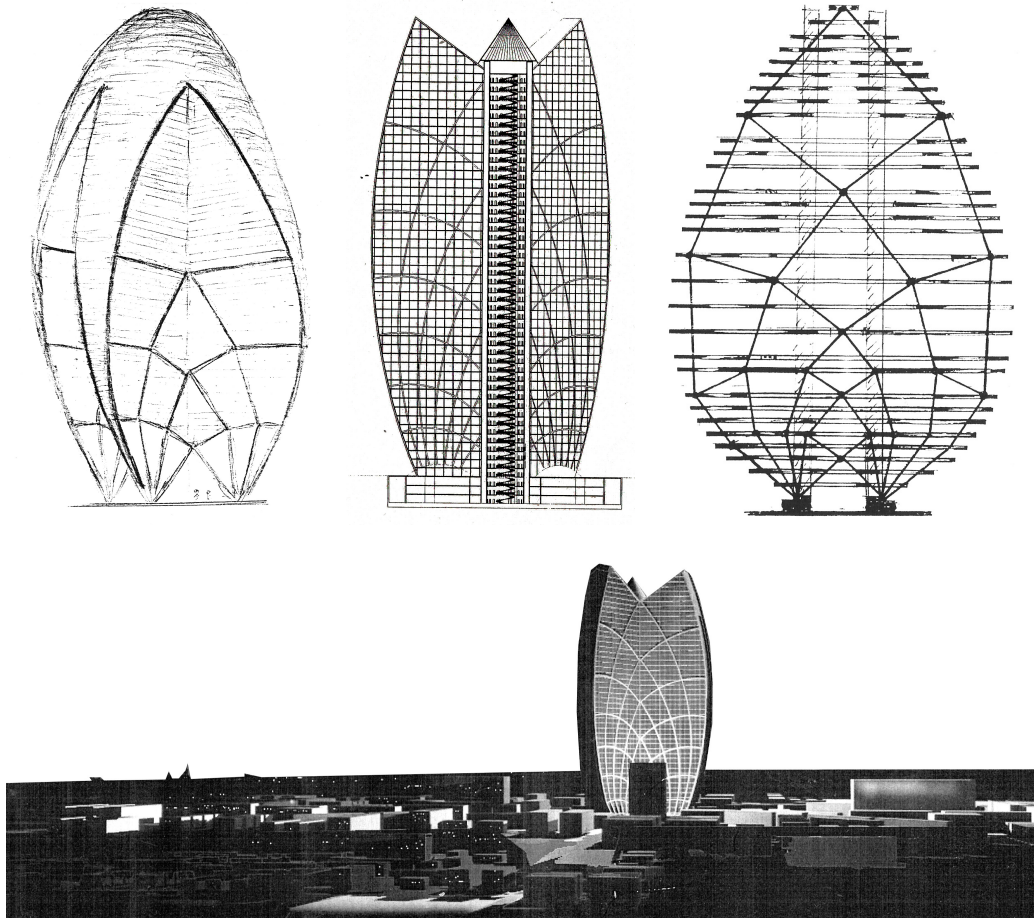
Figure 1-6: High-rise buildings inspired by 2D Michell structures, from [9].

1.2.2 Other applications

Other fields than structural engineering have shown interest for Michell structures in the past. In aeronautical and aerospace engineering for example, NASA produced technical documentation [11] in 1968 on how to implement Michell theory in aeronautics structures. Three-dimensional Michell structures may therefore be of interest for this field and for the design of wings especially, as such elements tend to be dominated by one unique load case induced by the difference of air pressure between their intrados (i.e. bottom side) and extrados (i.e. top side).

Other applications of interest for three-dimensional Michell structures are about making more economical supports for oil rigs or transmission towers. For both cases,

economies in material may be in the same order of magnitude. If supports for oil rigs consist in one big structure, transmission towers are indeed smaller structures that are duplicated all along an electric network.

Figure 1-7: Other potential applications for 3D Michell structures.

1.3   Problem statement

The problem statement of this thesis is straightforward: how can three-dimensional Michell structures be generated?

To answer this question, the research is broken into several steps, presented in this thesis in the order shown below:

- The first objective of this research is to understand Michell theory in two dimensions, which comprises the first part of Chapter 2, *Literature review.*

- The second step is to understand the challenges existing theory poses for the generation of three-dimensional Michell structures. This comprises the second part of Chapter 2, *Literature review.*

- The third step consists in defining a new mathematical approach that facilitates the generation of 3D structures, and prove that such an approach is consistent with the existing 2D theory. This step is further developed in Chapter 3, *Theory and methodology.*

- The fourth step is then to ensure in practice that the new method was consistent with known 2D Michell structures, which is shown in 4, *Results in 2D.*

- Finally, the last step of this research is to use the new mathematical approach to regenerate the only well-known 3D Michell structure so far and, then, to generate new 3D Michell structures. This step is discussed in Chapter 5, *Results in 3D*.

1.4 Terminology

Throughout this thesis, some words will appear quite often. To avoid any misunderstanding, let's define them:

- Structure: it is a set of lines that undergo tension or compression forces only when resisting given loading conditions.

- Optimum structure: it is a structure which is of minimum weight relative to other structures resisting the same loading conditions, and relative to the planar or spatial domain Ω in which the structures are allowed to exist.

- Strain tensor: it is a matrix representation of the distribution of strain within a planar (2×2 matrix) or spatial domain (3×3 matrix) Ω. It is a function of the coordinate system variables and returns the strain in any direction $\boldsymbol{d}$ and at any point $M \in \Omega$, when taking the coordinates of $\boldsymbol{d}(M)$ as input. Its analytical expression varies with the basis and the coordinate system, but the norm and directions of the strain vectors it returns remain always the same.

- Strain field: it is a graphical representation of the distribution of strain within a planar or spatial domain Ω. It shows vectors of strain at any point $M \in \Omega$, hence showing the amplitudes of strain in every directions and in every location within Ω.

  N.B.: Strain tensor and strain fields carry the exact same information. In essence, they are the same thing.

- Principal strains: they refer to both the eigenvalues and eigenvectors of a given strain tensor.

Also, variables displayed in **bold** will refer to multivariate variables, i.e. vectors and matrices.

Chapter 2

Literature review

This chapter is an examination of several important contributions in the development of Michell structures. First, the fundamental theory contributed by Maxwell[12] will be investigated. Then, Michell's seminal paper[1] will be analyzed. Finally, research of interest for three-dimensional Michell structures will be reviewed.

2.1   Maxwell's theorem

2.1.1   Statement

One could think structural optimization is quite recent, as one assumes it heavily relies on computers. It is actually not true, as one of the key figures in the history of structural optimization is James Clerk Maxwell himself (1831 - 1879). In 1870, Maxwells notes were published and some of them dealt with structural mechanics[12]. More precisely, Maxwell studied the properties of trusses and found a fundamental equation verified by any truss submitted to one same system of applied forces:

$$\sum F_t L_t - \sum F_c L_c = C \tag{2.1}$$

Where:

- L_t and L_c are the length of a member, whether it is under tension (t) or compression (c).

- F_t and F_c are the norms of the internal tension or compression forces.

- C is a constant independent of the truss.

It is noticeable that the above equation is equivalent to:

$$\sum \sigma_t V_t - \sum \sigma_c V_c = C \tag{2.2}$$

Where:

- σ_t and σ_c are the stress in a member under tension or compression.

- V_t and V_c are the volume of a member under tension or compression.

- C is the same constant as in 2.1.

The main interest of this theorem is that no matter the shape of the truss resisting a given loading - such as $\boldsymbol{F_1}$, $\boldsymbol{F_2}$, $\boldsymbol{F_3}$, $\boldsymbol{F_4}$, $\boldsymbol{F_5}$ in figure 2-1 -, the same constant C is found when multiplying the length of each truss member by its respective internal force and summing for every truss member. Therefore, even though trusses 1, 2 or 3 are geometrically very different in figure 2-1, the difference in their tension and compression load paths is always equal to C.

2.1.2 Proof for 2D

As shown in Maxwell's statement, the left member of Maxwell's equation depends on the truss, whereas the right one does not. The latter only depends on the applied forces, as the following proof will explain. Even though Maxwell himself gives the idea of this proof, he doesn't explicitly formulate it in mathematical terms, but as shown in figure 2-2. In order to better understand Maxwell's proof, an illustration of figure 2-2 is shown in figure 2-3. The steps in figure 2-3 correspond to:
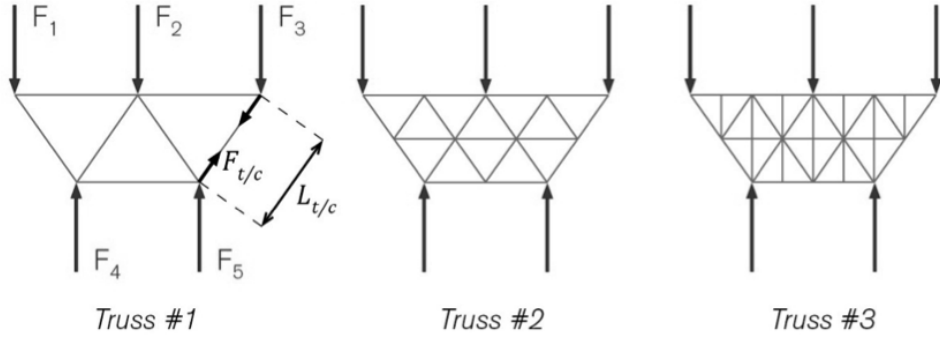
$$\left(\sum L_t F_t - \sum L_c F_c\right)_{Truss\ \#1} = \left(\sum L_t F_t - \sum L_c F_c\right)_{Truss\ \#2} = \left(\sum L_t F_t - \sum L_c F_c\right)_{Truss\ \#3} = C$$

Figure 2-1: Maxwell's theorem for different trusses submitted to a similar loading.

> For since each point is in equilibrium under the action of a system of attractions and repulsions in one plane, it will remain in equilibrium if the system of forces is turned through a right angle in the positive direction. If this operation is performed on the systems of forces acting on all the points, then at the extremities of each line joining two points we have two equal forces at right angles to that line and acting in opposite directions, forming a couple whose magnitude is the product of the force between the points and their distance, and whose direction is positive if the force be repulsive, and negative if it be attractive. Now since every point is in equilibrium these two systems of couples are in equilibrium, or the sum of the positive couples is equal to that of the negative couples, which proves the theorem.

Figure 2-2: Maxwell's 2D proof, from [12].

1. **Step 1**: Let's consider a random truss, submitted to a certain loading $\{F_1, F_2, F_3, F_4, F_5\}$. It is noticeable that this loading actually includes both applied forces $\{F_1, F_2, F_3\}$ and support reactions $\{F_4, F_5\}$. The internal forces are denoted by $F_{t,i}$ if the member "i" is under tension, and $F_{c,j}$ if the one denoted as "j" is under compression.

2. **Step 2**: Probably because Maxwell has done so much in the field of electromagnetism, he actually considers a truss by its nodes. These nodes are connecting the truss members together and are therefore submitted to whatever force $F_{t,i}$ or $F_{c,j}$ each member they are connected to has. Such a way of seeing things is interesting, as there is not much difference left between a truss and a set of magnets under attraction or repulsion the ones with the others. The only
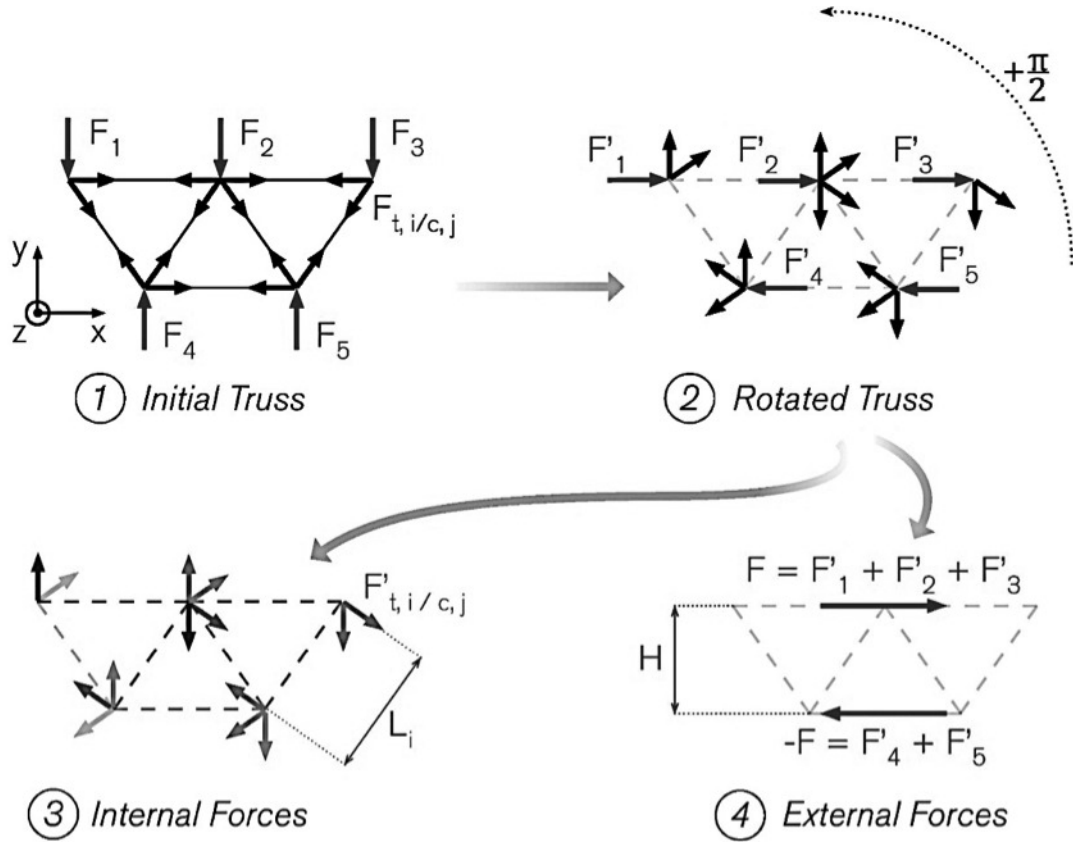
Figure 2-3: Sketch for Maxwell's proof in 2D.

difference is actually semantic, as attraction would correspond to compression, whereas repulsion to tension.

That being said, whatever planar rotation R_θ you apply to the forces of the set of nodes, global equilibrium will be maintained. Indeed, if the initial truss is both at internal and external equilibrium, then, for each node N:

$$\sum_{i\in I} \boldsymbol{F_{t,i}} + \sum_{j\in J} \boldsymbol{F_{c,j}} + \sum_{k\in K} \boldsymbol{F_k} = \boldsymbol{0} \qquad (2.3)$$

Where:

- $I = \{i_0; i_1; \dots; i_n\}$ refers to members under tension meeting at node N.

- $J = \{j_0; j_1; \dots; j_m\}$ refers to members under compression meeting at node N.

- K refers to all the external forces applied at node N.

Then:

$$R_\theta\left(\sum_{i\in I}\boldsymbol{F_{t,i}}+\sum_{j\in J}\boldsymbol{F_{c,j}}+\sum_{k\in K}\boldsymbol{F_k}\right)=R_\theta\left(\boldsymbol{0}\right)=\boldsymbol{0} \tag{2.4}$$

as R_θ is linear, and having $R_\theta(\boldsymbol{F})=\boldsymbol{F'}$, the above equation can be rewritten as:

$$\sum_{i\in I}\boldsymbol{F'_{t,i}}+\sum_{j\in J}\boldsymbol{F'_{c,j}}+\sum_{k\in K}\boldsymbol{F'_k}=\boldsymbol{0} \tag{2.5}$$

The rotated truss in step 2 of figure 2-1 is hence the result of a counterclockwise rotation of angle $\frac{\pi}{2}$ applied to every node, $R_{\frac{\pi}{2}}$.

3. **Step 3**: The new internal loads $\boldsymbol{F'_{t,i}}$ or $\boldsymbol{F'_{c,j}}$ are perpendicular to the truss members denoted as "i" or "j". Hence, moments have been virtually created. Each member "i" or "j" is now submitted to a couple equal to $C_{t,i}$ or $C_{c,j}$, with:

$$\begin{cases}C_{t,i}=+L_i\|\boldsymbol{F'_{t,i}}\|\boldsymbol{u_z}=+L_i\|\boldsymbol{F_{t,i}}\|\boldsymbol{u_z}\\ C_{c,j}=+L_j\|\boldsymbol{F'_{c,j}}\|\boldsymbol{u_z}=+L_j\|\boldsymbol{F_{c,j}}\|\boldsymbol{u_z}\end{cases} \tag{2.6}$$

Where:

- $\|.\|$ is the Euclidean norm.

- $\boldsymbol{u_z}$ denotes the third space direction relatively to figure 2-1

In figure 2-1, each couple $C_{t,i}$ or $C_{c,j}$, is shown with a proper grey tone and consists in two equal and opposed forces. Moreover, as stated in equation 3.20, $\|\boldsymbol{F'}\|=\|\boldsymbol{F}\|$ as $R_{\frac{\pi}{2}}$ preserves the norm.

4. **Step 4**: Calculating the moments created by external forces $\{\boldsymbol{F'_1},\ \boldsymbol{F'_2},\ \boldsymbol{F'_3},\ \boldsymbol{F'_4},\ \boldsymbol{F'_5}\}$ is equivalent to adding all the applied forces together and adding all the reaction forces together. Therefore:

$$\begin{cases}\boldsymbol{F}&=\sum_{k\in K_1}\boldsymbol{F'_k}\\ -\boldsymbol{F}&=\sum_{k\in K_2}\boldsymbol{F'_k}\end{cases} \tag{2.7}$$

Where:

- K_1 refers to the indices of all the external applied forces.

- K_2 refers to the indices of all the external support reactions.

The reason the first equation in 2.7 is the opposite of the second equation in 2.7 is due to the global action versus reaction equilibrium. And once again, a couple has been virtually created:

$$C_{ext} = -\|\boldsymbol{F}\|H\boldsymbol{u_z} \tag{2.8}$$

Where:

- C_{ext} is the couple caused by the external loading.

- H is as shown in figure 2-1.

For this specific case, equation 2.8 is true and can actually be extrapolated to many other cases.

5. **Step 5**: We now have all the tools to conclude and hence prove Maxwell's statement. We know that if the initial truss from step 1 is at equilibrium, then the rotated truss from step 2 is also at equilibrium. Therefore, we can write the moment equilibrium for the rotated truss, which is:

$$\sum_i C_{t,i} + \sum_j C_{c,j} + C_{ext} = 0 \tag{2.9}$$

i.e., per equations 2.6 and 2.8:

$$\left(\sum_i L_i\|\boldsymbol{F_{t,i}}\| + \sum_j L_j\|\boldsymbol{F_{c,j}}\| - \|\boldsymbol{F}\|H \right) \boldsymbol{u_z} = 0 \tag{2.10}$$

Analogy with Maxwell's statement is then proved. Comparing equations 2.10 with 2.1, we indeed have:

- L_i or L_j corresponding to L_t or L_c.

- $\|\boldsymbol{F_{t,i}}\|$ or $\|\boldsymbol{F_{c,j}}\|$ corresponding to F_t or Fc.

- $\|\boldsymbol{F}\|H$ corresponding to C.

2.1.3 Proof for 3D

Maxwell also gives a proof for the 3D case of his theorem, i.e. when the loading and truss under consideration are defined in the three directions of space. This time, Maxwell formulates his proof as shown in figure 2-4, which is graphically explained in figure 2-5. What happens at each step is as follows:

1. **Step 1**: The truss is now a 3D one, with bars laid out in every three directions of space. As for the 2D proof, we consider a random truss, submitted to a certain loading $\{F_1, F_2, F_3, F_4, F_5\}$. In the sake for clarity, internal forces are denoted differently than in figure 2-1. Here, the force at node i that binds the latter with node j is denoted as F_{ij}.

2. **Step 2**: Maxwell wants the truss to contract up to a single point. Defining this point as the origin of a Cartesian frame (O, e_x, e_y, e_z), the contraction can now be seen as a movement of each node from its initial position in the truss to O. Moreover, each force being a conservative force, there is no need to know what the contraction path is.

   The work performed by each force in a single direction of space, say x, is hence:

$$W_{ij,x} = \int_O^j \langle F_{ij} | e_x \rangle dx = \|F_{ij}\| cos(\theta_{ij}) x_i \tag{2.11}$$

   Where:

   - $\langle ... | ... \rangle$ is the Euclidean dot product.
   - F_{ij} is the force at node i, due to its interaction with point j.
   - $W_{ij,x}$ is the work of F_{ij} in the x direction.
   - θ_{ij} is the angle between the x axis and the bar joining nodes i and j together.
   - r_{ij} is the distance between nodes i and j.

   Also, by symmetry:

$$W_{ji,x} = \|F_{ij}\| \frac{(x_i - x_j)}{r_{ij}} x_j = -\|F_{ij}\| \frac{(x_j - x_i)}{r_{ij}} x_j \tag{2.12}$$

The following method of demonstrating this theorem does not require the consideration of couples, and is applicable to frames in three dimensions.

Let the system of points be caused to contract, always remaining similar to its original form, and with its pieces similarly situated, and let the same forces continue to act upon it during this operation, so that every point is always in equilibrium under the same system of forces, and therefore no work is done by the system of forces as a whole.

Let the contraction proceed till the system is reduced to a point. Then the work done by each tension is equal to the product of that tension by the distance through which it has acted, namely, the original distance between the points. Also the work spent in overcoming each pressure is the product of that pressure by the original distance of the points between which it acts; and since no work is gained or lost on the whole, the sum of the first set of products must be equal to the sum of the second set. In this demonstration it is not necessary to suppose the points all in one plane. This demonstration is mathematically equivalent to the following algebraical proof:—

Let the co-ordinates of the n different points of the system be $x_1 y_1 z_1$, $x_2 y_2 z_2$, $x_p y_p z_p$, &c., and let the force between any two points p, q, be P_{pq}, and their distance r_{pq}, and let it be reckoned positive when it is a pressure, and negative when it is a tension, then the equation of equilibrium of any point p with respect to forces parallel to x is

$$(x_p - x_1)\frac{P_{p1}}{r_{p1}} + (x_p - x_2)\frac{P_{p2}}{r_{p2}} + \&c. + (x_p - x_q)\frac{P_{pq}}{r_{pq}} + \&c. = 0,$$

or generally, giving t all values from 1 to n,

$$\Sigma_1^n t \left\{ (x_p - x_t)\frac{P_{pt}}{r_{pt}} \right\} = 0.$$

Multiply this equation by x_p. There are n such equations, so that if each is multiplied by its proper co-ordinate and the sum taken, we get

$$\Sigma_1^n p \, \Sigma_1^n t \left\{ (x_p - x_t)^2 \frac{P_{pt}}{r_{pt}} \right\} = 0,$$

and adding the corresponding equations in y and z, we get

$$\Sigma_1^n p \, \Sigma_1^n t \, (P_{pt} r_{pt}) = 0,$$

which is the algebraic expression of the theorem.

Figure 2-4: Maxwells explanations for 3D, from [12]

Let's add equations 2.11 and 2.12:

$$W_{ij,x} + W_{ji,x} = \|\boldsymbol{F_{ij}}\|\frac{(x_j - x_i)}{r_{ij}}x_i - \|\boldsymbol{F_{ij}}\|\frac{(x_j - x_i)}{r_{ij}}x_j = -\frac{\|\boldsymbol{F_{ij}}\|}{r_{ij}}(x_j - x_i)^2 \quad (2.13)$$

Neglecting the truss self weight, the kinetic energy of the nodes displacement is
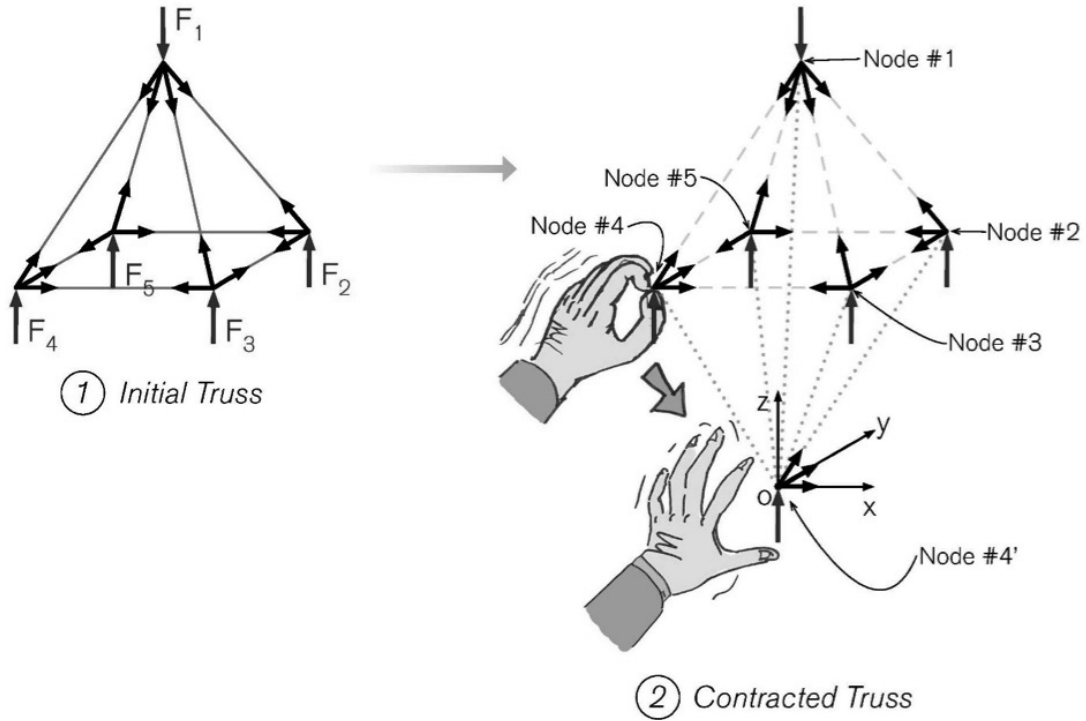
Figure 2-5: Sketch for Maxwells proof in 3D

set equal to zero, as these nodes dont have any mass. Therefore, by applying the theorem of kinetic energy:

$$\sum_{i<j} W_{ij,x} + W_{ji,x} = 0 \tag{2.14}$$

Extrapolating this result for each three directions of space, equations 2.13 and 2.14 give:

$$\begin{cases} \sum_{i<j} \dfrac{\|\boldsymbol{F_{ij}}\|}{r_{ij}}(x_j - x_i)^2 & = 0 \\[2mm] \sum_{i<j} \dfrac{\|\boldsymbol{F_{ij}}\|}{r_{ij}}(y_j - y_i)^2 & = 0 \\[2mm] \sum_{i<j} \dfrac{\|\boldsymbol{F_{ij}}\|}{r_{ij}}(z_j - z_i)^2 & = 0 \end{cases} \tag{2.15}$$

And hence, by adding all three equations of 2.15:

$$\sum_{i<j} \|\boldsymbol{F_{ij}}\| r_{ij} = 0 \tag{2.16}$$

Equation 2.16 is therefore identical to Maxwell's theorem, which ends the proof.

2.1.4   Remarks

As stated by Baker[13], Maxwell's theorem and equation 2.1 show us that any wrong positioning of a member in a truss will be paid twice in terms of use of material. If a tension (or compression) part of the structure does not have the optimal geometrical layout in terms of volume, it will have to be counterbalanced by an increase in the compression (or tension) term in 2.1 so as for the subtraction to remain equal to the C constant. The need for properly positioning truss members is hence crucial for a project to be recognized as a material-efficient one.

In that respect, we now introduce Michell's theorems, that will greatly help in the design of such an optimal layout.

2.2   Michell's theorems

Even though Michell's seminal paper[1] describes what conclusions can be drawn from Maxwell's theorem for the first time, other authors have further explained how to come to such conclusions, such as Spillers[14] or Lewinski[15].

We here reproduce Spillers' subdivision of Michell's approach in three theorems, as it is clear and straightforward at the same time.

2.2.1 First theorem

Amid a set of structures verifying Maxwell's theorem for a given loading and support case, optimum structures will be the ones that minimize:

$$V_t f_t + V_c f_c$$

Where:

- V_t and V_c correspond to the total volume of tension and compression members respectively.

- f_t and f_c correspond to the maximal allowable stress for tension and compression.

Indeed, the total volume V of the structure is such that:

$$V = V_t + V_c = \frac{1}{2}\left(\left(\frac{1}{f_t} + \frac{1}{f_c}\right)(V_t f_t + V_c f_c) + \left(\frac{1}{f_t} - \frac{1}{f_c}\right)(V_t f_t - V_c f_c)\right) \quad (2.17)$$

Maxwell's theorem stating that $V_t f_t - V_c f_c$ is a constant, a structure minimizing V is a structure minimizing $V_t f_t + V_c f_c$.

2.2.2 Second theorem and Michell's rule

The quantity $V_t f_t + V_c f_c$ verifies:

$$V_t f_t + V_c f_c \geq \frac{W}{\varepsilon}$$

Where:

- W corresponds to the work of external forces.

- ε is the maximal strain in the structure: $\varepsilon = \max_i \left\|\frac{\boldsymbol{\Delta_i}}{L_i}\right\| = \max_i(\varepsilon_i)$, where i refers to a given truss member.

- $\boldsymbol{\Delta_i}$ is the axial displacement of member i.

- L_i is the length of member i.

The proof relies on applying the principle of virtual work to the given truss:

$$
\begin{aligned}
W &= W_{int} \\
&= \sum \langle \boldsymbol{F_i} | \boldsymbol{\Delta_i} \rangle = \sum \sigma_i A_i \varepsilon_i L_i = \sum \sigma_i \varepsilon_i V_i \\
&\leq f_c \sum_{j \in C} \varepsilon_j V_j + f_t \sum_{k \in T} \varepsilon_k V_k \\
&\leq \varepsilon (V_t f_t + V_c f_c)
\end{aligned}
\tag{2.18}
$$

Where W_{int} is the internal work of the truss. We conclude and find:

$$
V_t f_t + V_c f_c \geq \frac{W}{\varepsilon}
\tag{2.19}
$$

It is noticeable that inequalities become equalities in equations 2.18 and 2.19 if:

1. Any member is stressed up to its maximal allowable stress:
   $\forall i \in C \cup T, \sigma_i = f_t$ or f_c

2. Axial strain is the same in absolute value, whatever the member:
   $\forall i \in C \cup T, \varepsilon_i = \varepsilon$

A structure verifying these two conditions is therefore optimum: it minimizes $V_t f_t + V_c f_c$ in equation 2.19 and conclusion follows after invoking Michell's first theorem. Michell hence relies on such conditions to build optimum structures. The typical volume of a Michell structure V_m for $f_t = f_c = \sigma$ is therefore:

$$
V_m = \frac{W}{\sigma \varepsilon}
\tag{2.20}
$$

It has actually been later shown that Michell structures are of minimal volume for $f_t = f_c$ only. This shortcoming has been implicitly shown for the first time in Hemp[7], and later explicitly by Rozvany[16][17]. It will be reviewed in the next section, *The mathematics of Michell structures*, and modified criteria on strains ε_i will be determined so as to have equalities in equations 2.18 and 2.19 when $f_t \neq f_c$.

In chapters 4 *Results in 2D* and 5 *Results in 3D* however, we will consider equal permissible stresses, such that $f_t = f_c = \sigma$. We indeed assume solutions to be built in steel, for which such equality is true. Also, if the loading conditions are reversed, members in tension become members in compression, and vice-versa. Therefore, equal stresses in tension and compression make a Michell structure being the optimal solution for a given loading and its opposed version at the same time.

2.2.3 Third theorem

This theorem states that an optimum structure has a maximum overall stiffness.

If we restrict the study to elasticity only, Hooke's law brings: $\varepsilon_i = \frac{f_{t,c}}{E}$. For the sake for clarity, we consider a simple load case scenario with one point load F, implying a displacement δ, such that $W = F\delta$. Therefore:

$$
\begin{aligned}
F\delta &= \sum \sigma_i \varepsilon_i V_i = f_c \sum_{j \in C} \varepsilon_j V_j + f_t \sum_{k \in T} \varepsilon_k V_k = \frac{f_c^2}{E} \sum_{j \in C} V_j + \frac{f_t^2}{E} \sum_{k \in T} V_k \\
&= \frac{f_c^2}{E} V_c + \frac{f_t^2}{E} V_t \\
&= \frac{1}{E} \left(f_t f_c (V_t + V_c) + (f_t - f_c)(V_t f_t - V_c f_c) \right)
\end{aligned}
\tag{2.21}
$$

Maxwell's theorem stating that $V_t f_t - V_c f_c$ is a constant, a minimum for $V = V_t + V_c$ also minimizes the external work $F\delta$, following equation 2.21. As external forces are a given, a structure of minimum volume actually minimizes the displacement δ. Hence, an optimum structure has maximal stiffness.

2.3 The mathematics of Michell structures

2.3.1 Developing strain fields that meet Michell's rule

The development of strain fields that meet Michell's rule follows a procedure developed by Chan[18] and Hemp[7]. Details about this procedure are given in section

3.2.2 *Hemp-Chan procedure.* This procedure has been followed in many publications about 2D Michell structures, as in Ghista et al.[11].

2.3.2 Enhancing Michell's rule for non-equal maximal tension and compression stresses

As introduced in section 2.2.2 *Second theorem and Michell's rule*, Michell structures are optimum solutions of a loading problem if tension and compression members have equal permissible stresses, i.e. $\sigma_c = \sigma_t$.

If $\sigma_c \neq \sigma_t$, principal strains for tension and compression ε_t and ε_c shall not be equal in absolute value anymore. Instead, they shall be such that:

$$\begin{cases} \varepsilon_t = \dfrac{\sigma\varepsilon}{\sigma_t} \\ \varepsilon_c = \dfrac{\sigma\varepsilon}{\sigma_c} \end{cases} \tag{2.22}$$

Where σ and ε are parameters that vary with the boundary conditions of a given problem.

This new criteria was found by Hemp[7], chapter 1 and explicitly developed in Rozvany[16] and Lewinsky[15]. It mostly consists in using Lagrange multipliers in equation 2.19 in order to transform the sign of inequality by that of equality.

Let's remember that the objective is to find the most economical structure able to resist a given set of external loads. Such set induces the external work W_{ext} and the principle of virtual work brings that any structure shall produce an internal work equal to W_{ext} in order to be admissible. Keeping the same notations as in sections 2.1 and 2.2, we hence want to solve the minimization under constrains shown in equation 2.23, where variables are the stresses σ_i. Ultimately, we want to find what equation the strains in every member ε_i respect for the structure to have a minimal volume.

$$\begin{cases} \text{Minimize} & V = \sum_i \dfrac{1}{\sigma_i} L_i F_i \\ \text{Such that} & W_{ext} = \sum_i \varepsilon_i(\sigma_i) L_i F_i \end{cases} \tag{2.23}$$

We solve such minimization with Lagrange multipliers. We now minimize the dual function:

$$
\begin{aligned}
\mathcal{L}(\lambda, \sigma_i) &= V + \lambda \left(W_{ext} - \sum_i \varepsilon_i(\sigma_i) L_i F_i \right) \\
&= \lambda W_{ext} + \sum_i L_i F_i \left(\frac{1}{\sigma_i} - \lambda \varepsilon_i(\sigma_i) \right)
\end{aligned}
\tag{2.24}
$$

The volume of one given structure will always be minimal for $\sigma_i = f_t$ or f_c, depending whether member i undergoes tension or compression. Indeed, the higher the permitted stress, the smaller the section area, therefore the smaller the volume.

Minimizing equation 2.24 is therefore equivalent to minimizing the following simplified version of the dual function:

$$
\mathcal{L}(\lambda, f_t, f_c) = \lambda W_{ext} + \sum_{i \in T} L_i F_i \left(\frac{1}{f_t} - \lambda \varepsilon_i(f_t) \right) + \sum_{j \in C} L_j F_j \left(\frac{1}{f_c} - \lambda \varepsilon_j(f_c) \right)
\tag{2.25}
$$

Because W_{ext} is a function of external loading only, it is not a function of f_t or f_c. Derivating equation 2.25 with respect to f_t brings:

$$
\frac{\partial \mathcal{L}}{\partial f_t} = \sum_{i \in T} L_i F_i \left(-\frac{1}{f_t^2} - \lambda \frac{\partial \varepsilon_i}{\partial f_t} \right)
\tag{2.26}
$$

A minimum is found for $\dfrac{\partial \mathcal{L}}{\partial f_t} = 0$, i.e.:

$$
\frac{\partial \varepsilon_i}{\partial f_t} = -\frac{1}{\lambda f_t^2}
\tag{2.27}
$$

Hence:

$$
\varepsilon_i = \frac{1}{\lambda f_t}
\tag{2.28}
$$

For the principle of homogeneity of dimensions to be more perceptible in equation 2.28, we can define the constant parameter λ by:

$$
\lambda = \frac{1}{\sigma \varepsilon}
\tag{2.29}
$$

Where σ and ε are two "correlated" parameters, the first being a stress, the second a

strain, and the value of both varying from one problem to another depending on the boundary conditions. Equation 2.28 becomes:

$$\varepsilon_i = \frac{\sigma\varepsilon}{f_t}, \ i \in T \tag{2.30}$$

Similarly, $\dfrac{\partial \mathcal{L}}{\partial f_c} = 0$ brings:

$$\varepsilon_j = \frac{\sigma\varepsilon}{f_c}, \ j \in C \tag{2.31}$$

Hence, equation 2.22 has been proved. Such conditions bring the best optimum volume for a structure, therefore a structure meeting such conditions shall be called Hemp structure, rather than Michell structure, following Rozvany's recommendation[16].

Let's note that such conditions are consistent with the condition of equal permissible strains in absolute value for $f_t = f_c = \sigma$.

Second, we will consider that $f_t = f_c = \sigma$ in chapters 4 *Results in 2D* and 5 *Results in 3D*. As explained previously, we indeed assume solutions to be built in steel, for which such equality is true.

Finally, performing Lagrangian optimization on both the equations of principle of virtual work and volume of a structure is a powerful approach in structural engineering in general. It was also used in Baker[19] to find the minimal volume of a given structure resisting a given loading, by varying the section areas A_i and finding what the analytical expression of W_{int} and W_{ext} was, accordingly to the load case under consideration.

Actually, as discussed in section 6.2 *Future work*, a potential future research direction would be to investigate how Hemp's optimum criteria shown in equation 2.22 varies when the structure becomes a moment frame (i.e. when bending is permitted). Inspiration could be found in Baker[19].

2.4 3D Michell structures

2.4.1 Topology optimization

Three-dimensional Michell structures have already been approximated through computational methods, especially numerical topology optimization. Numerical tools give an idea on how three dimensional Michell structure look, but are unable to prove that such a shape is the only solution.

As noted by Jouve[20], structural optimization problems are typically ill-posed problems. It means that there is not always existence of solutions. If a solution exists, it may also not be unique - see for example Mazurek et al.[21] for a multi-solution two-dimensional problem known as the "tri-force".

Such ill-posedness is therefore quite an issue for computer-based optimization methods. For example, if an algorithm is conceived so as to take a certain loading as input and to display the corresponding optimum structure as output, there is a risk for the algorithm to be trapped in a local minima and not see the possible many other solutions of the problem. Also, it may not find any solution at all. And finally, this algorithm will be likely to be unstable if the domain of optimization is discontinuous. Computational enhancements, however, exist to address such issues, according to Jouve[20] and Zegard & Paulino[22]. Despite the aforementioned shortcomings, beautiful structures have been found through topology optimization, in particular in Victoria et al.[23] (see figures 2-6a and 2-6b) and Zegard & Paulino[22] (see figure 2-6c).

2.4.2 A criteria for 3D Michell structures

If most of what is known so far for three-dimensional Michell structures is based on computational methods, fundamental analytical results have been found by Lewinski & Sokol[15]. Starting with the calculations shown in section 2.3.2 *Enhancing Michell's rule for non-equal maximal tension and compression stresses*, the authors derive the following criteria for three-dimensional structures to be considered as Michell struc-
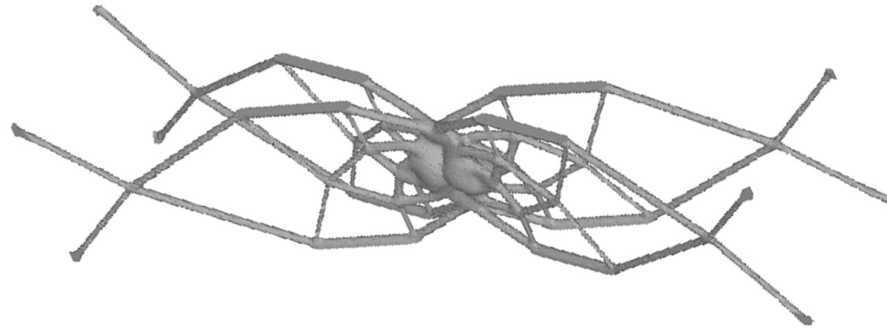
(a) An embedded cantilever beam, from [23].
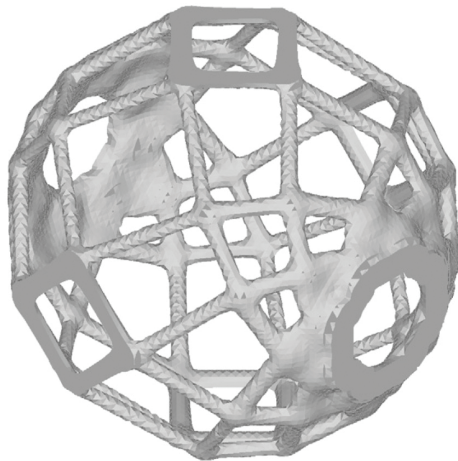
(b) A numerical approximation of Michell's sphere, from [23].

(c) Another numerical approximation of Michell's sphere, from [22].

Figure 2-6: 3D structures from topology optimization.

tures:

"*If the strain lies between the bounds [ε_c and ε_t], the fibres do not work; they began to work if the strains attain the bounds. In 3D if both bounds are attained, then the intermediate principal strain lies between the bounds and hence the corresponding stress vanishes. This means that there are no fibres in the direction of the intermediate principal direction and since the strains in other directions than I* [direction with higher principal strain] *and III* [direction with lower principal strain] *vanish, the only fibers lie along the I and III directions. The optimal structure becomes a fibrous shell in the membrane state of stress; the normal direction to this shell is the direction II.*"

Therefore, three-dimensional Michell structures can be generated in three-dimensions with the following criteria, that will be referred as Lewinsky's criteria in the rest of this thesis: a three-dimensional Michell structure can be generated from a three-dimensional strain field as soon as the latter has a maximal eigenvalue (or maximal principal stress) constantly equal to $\varepsilon > 0$ and a minimal eigenvalue (or minimal principal stress) constantly equal to $-\varepsilon$.

As explained before, we indeed consider maximal allowable stresses in tension or compression, hence equal strains for tension and compression in absolute value.

2.5 Limitations of existing work

In three dimensions, numerical topology optimization is the only reliable option to approximate Michell structures for new loading conditions. It is therefore a powerful tool to gain a sense of how Michell structures will look.

However, it is nevertheless unsatisfying not to have the exact analytical expression of the true optimum Michell structure through this method. For example, topology optimization is not able to find the functional expression of the lines of a three-dimensional Michell structure. By itself, it is also unable to find the functional expression of the volume V_m of the Michell structure it approximates.

Following the methodology from Zegard & Paulino[22], a structure found through topology optimization is a good approximation of a Michell structure if its volume is close enough to V_m, implying that V_m is known. Hence, analytical solutions of three-dimensional problems shall be determined so as to give the value V_m, and, more broadly, a full analytical description of a given Michell structure.

THIS PAGE INTENTIONALLY LEFT BLANK

Chapter 3

Theory and methodology

As a brief summary of last chapter, Michell[1], shows structures of minimal weight for different loading conditions but the procedure to be used in order to generate such shapes remains unclear. Decades later, in the 1960s and 1970s, mathematicians such as Chan[18] or Hemp[7] have further investigated Michell structures and have been able to define a detailed mathematical procedure to draw them, providing a better understanding of such structures at the same time.

Such procedures work perfectly and elegantly in two-dimensional cases, but they can't be generalized to three dimensional cases. In Hemp[7] for example, the mathematical procedure shares similarities with complex variable theory - see Sadd[24], chapter 10 for complete introduction of this theory. Complex variables are powerful objects to simplify the analysis of two dimensional problems, by integrating one direction of the plane in their real part and the other in their imaginary part. But this power in 2D becomes weakness in 3D, as there is no room left for the third spatial direction to be integrated in a complex variable.

Therefore, a new method needs to be developed in order to generate three dimensional Michell structures. This chapter introduces such a new method: the Michell strain tensor method, or MSTM.

Instead of complex variable theory, MSTM follows the general principles of elasticity to build strain fields. However, it disregards the laws of elasticity that force a strain

field to induce equilibrium within a continuous body. MSTM rather forces the strain field to meet Michell's rule or Lewinsky's criteria, as introduced in sections 2.2.2 and 2.4.2 respectively.

3.1   Principles of MSTM

Let's have a generic orthogonal curvilinear coordinate system (α, β, γ), whose basis vectors are $(\boldsymbol{e_\alpha}, \boldsymbol{e_\beta}, \boldsymbol{e_\gamma})$. These six variables are all functions of the Cartesian coordinates (x, y, z).

By Sadd[24], equations (2.2.7), the strain field (or tensor) $\boldsymbol{\varepsilon}$ corresponding to a small displacement $\boldsymbol{u}(\alpha, \beta, \gamma) \in \mathscr{C}^1(\mathbb{R}^3, \mathbb{R}^3)$ is:

$$\boldsymbol{\varepsilon} = \frac{1}{2} \left(\boldsymbol{\nabla u} + \boldsymbol{\nabla u}^\mathsf{T} \right) \tag{3.1}$$

Where $\boldsymbol{\nabla u}$ is the gradient matrix associated to $\boldsymbol{u}$. Also, a displacement is considered small when its magnitude is of much lower order than the typical dimensions of the structure. There is no loss of generality by making the assumption of small displacements, as the structure shall be usable anyway. Also, equation 3.1 holds for any orthogonal curvilinear coordinate system - see Love[25], equation 36. It follows that a strain field can be found for any displacement $\boldsymbol{u} \in \mathscr{C}^1(\mathbb{R}^3, \mathbb{R}^3)$.

Information on $\boldsymbol{u}$ makes the calculation of $\boldsymbol{\varepsilon}$ in equation 3.1 easier. Knowing which of the basis variables and vectors $\boldsymbol{u}$ is the function of indeed simplifies its expression. $\boldsymbol{u}$ can also be simplified so as to fit to the geometry of the problem and to respect the boundary conditions. Using equation 3.1, we then derive an expression for $\boldsymbol{\varepsilon}$.

In $\mathbb{R}^2$, $\boldsymbol{\varepsilon}$ needs to have constant and equal eigenvalues in absolute value to meet Michell's rule, as introduced in 2.2.2 *Second theorem and Michell's rule*. Implementing this condition on $\boldsymbol{\varepsilon}$ and $\boldsymbol{u}$, we shall find their corresponding analytical expressions.

In $\mathbb{R}^3$, the maximal and minimal eigenvalues of $\boldsymbol{\varepsilon}$ need to be constant and equal in absolute value to meet Lewinsky's criteria, as introduced in 2.4.2 *A criteria for 3D Michell structures*. Again, we shall find the analytical solution for $\boldsymbol{\varepsilon}$ and $\boldsymbol{u}$ by

implementing this condition.

Now that $\boldsymbol{\varepsilon}$ is analytically determined, its corresponding Michell structure can be drawn, relying on what the eigenvectors of $\boldsymbol{\varepsilon}$ are.

3.2 Proof of equivalence between MSTM in 2D and Hemp & Chan procedure

First, let's define a 2D orthogonal curvilinear coordinate system S whose variables are (α, β) and basis vectors are $(\boldsymbol{e_\alpha}, \boldsymbol{e_\beta})$. Variables and basis vectors of S are all functions of the plane coordinates. We also define Ω as being the region of plane in which the potential Michell structures are allowed to exist.

In either Chan[18], equation 10, or Hemp[7], equation 4.22, Michell structures[1] are generated based on an angular potential ϕ_0, solution of:

$$\frac{\partial^2 \phi_0}{\partial \alpha \partial \beta} = 0 \tag{3.2}$$

Equation 3.2 is fundamental in Hemp or Chan in the sense that this is the starting point when solving a given problem. By solving equation 3.2 for the given problem conditions, the corresponding Michell structure is found. Equation 3.2 is actually explicitly recognized as the characterization of Michell structures in Chan[18], Hemp[7] or Strang & Kohn[26].

The intent of this proof is to understand how equation 3.2 is found, and to see if MSTM follows the same logical steps - it will actually be shown that it does follow the same steps, but not in the same order, which leads to equivalent results anyway.

In the plane, we keep the orthogonal curvilinear system S introduced above and we consider the displacement $\boldsymbol{u}$:

$$\boldsymbol{u} = u_\alpha \boldsymbol{e_\alpha} + u_\beta \boldsymbol{e_\beta} \tag{3.3}$$

---

[1]The term "Michell structure" is correct when referring to Hemp if we have $f_t = f_c = \sigma$, as explained in sections 2.2.2 and 2.3.2. Following Rozvany's recommendation [16], we shall otherwise use the term "Hemp structure".

Let's now build the strain field corresponding to $\boldsymbol{u}$. Following Sadd[24], section 1.9, the basis vectors of S are such that:

$$
\begin{cases}
\dfrac{\partial \boldsymbol{e_\alpha}}{\partial \alpha} = -\dfrac{1}{B}\dfrac{\partial A}{\partial \beta}\boldsymbol{e_\beta} \\[2ex]
\dfrac{\partial \boldsymbol{e_\alpha}}{\partial \beta} = \dfrac{1}{A}\dfrac{\partial B}{\partial \alpha}\boldsymbol{e_\beta} \\[2ex]
\dfrac{\partial \boldsymbol{e_\beta}}{\partial \beta} = -\dfrac{1}{A}\dfrac{\partial B}{\partial \alpha}\boldsymbol{e_\alpha} \\[2ex]
\dfrac{\partial \boldsymbol{e_\beta}}{\partial \alpha} = \dfrac{1}{B}\dfrac{\partial A}{\partial \beta}\boldsymbol{e_\alpha}
\end{cases}
\tag{3.4}
$$

Where A and B are the scale factors of S in the respective directions $\boldsymbol{e_\alpha}$ and $\boldsymbol{e_\beta}$ and are functions of the plane coordinates. In order to make equation 3.4 more understandable, let's show that the derivatives of a basis vector are necessarily orthogonal to the basis vector itself. As:

$$
\langle \boldsymbol{e_\alpha} | \boldsymbol{e_\alpha} \rangle = 1
\tag{3.5}
$$

Where $\langle ...|... \rangle$ is the Euclidean dot product. We find:

$$
\frac{\partial}{\partial \beta}\langle \boldsymbol{e_\alpha}|\boldsymbol{e_\alpha}\rangle = 2\langle \frac{\partial \boldsymbol{e_\alpha}}{\partial \beta}|\boldsymbol{e_\alpha}\rangle = 0
\tag{3.6}
$$

Which holds true whatever the indices.

Back to the proof, equations 3.3 and 3.4 are then applied to the definition of the gradient matrix in curviliear coordinates, so that:

$$
\boldsymbol{\nabla u} =
\begin{pmatrix}
\dfrac{1}{A}\dfrac{\partial u_\alpha}{\partial \alpha} + \dfrac{1}{AB}\dfrac{\partial A}{\partial \beta}u_\beta & \dfrac{1}{A}\dfrac{\partial u_\beta}{\partial \alpha} - \dfrac{1}{AB}\dfrac{\partial A}{\partial \beta}u_\alpha \\[3ex]
\dfrac{1}{B}\dfrac{\partial u_\alpha}{\partial \beta} - \dfrac{1}{AB}\dfrac{\partial B}{\partial \alpha}u_\beta & \dfrac{1}{B}\dfrac{\partial u_\beta}{\partial \beta} + \dfrac{1}{AB}\dfrac{\partial B}{\partial \alpha}u_\alpha
\end{pmatrix}
\tag{3.7}
$$

Also, let us notice the following equality:

$$
\frac{1}{A}\frac{\partial u_\beta}{\partial \alpha} - \frac{1}{AB}\frac{\partial B}{\partial \alpha}u_\beta + \frac{1}{B}\frac{\partial u_\alpha}{\partial \beta} - \frac{1}{AB}\frac{\partial A}{\partial \beta}u_\alpha = \frac{B}{A}\frac{\partial}{\partial \alpha}\left(\frac{u_\beta}{B}\right) + \frac{A}{B}\frac{\partial}{\partial \beta}\left(\frac{u_\alpha}{A}\right)
\tag{3.8}
$$

Using equations 3.1, 3.7 and 3.8, the strain tensor is:

$$
\varepsilon = \begin{pmatrix} \dfrac{1}{A}\dfrac{\partial u_\alpha}{\partial \alpha} + \dfrac{1}{AB}\dfrac{\partial A}{\partial \beta}u_\beta & \dfrac{1}{2}\left(\dfrac{B}{A}\dfrac{\partial}{\partial \alpha}\left(\dfrac{u_\beta}{B}\right) + \dfrac{A}{B}\dfrac{\partial}{\partial \beta}\left(\dfrac{u_\alpha}{A}\right)\right) \\[3mm] \dfrac{1}{2}\left(\dfrac{B}{A}\dfrac{\partial}{\partial \alpha}\left(\dfrac{u_\beta}{B}\right) + \dfrac{A}{B}\dfrac{\partial}{\partial \beta}\left(\dfrac{u_\alpha}{A}\right)\right) & \dfrac{1}{B}\dfrac{\partial u_\beta}{\partial \beta} + \dfrac{1}{AB}\dfrac{\partial B}{\partial \alpha}u_\alpha \end{pmatrix} \tag{3.9}
$$

Now is the point where Hemp-Chan procedure differs from MSTM. Let's have a subsection for each approach, and then conclude.

3.2.1 Michell strain tensor method

In MSTM, we find a strain tensor ε the same way we did so far in the proof, with initial assumptions on $\boldsymbol{u}$ to make the calculations of equations 3.7 and 3.10 simple (but nevertheless keeping in mind we need to find a solution to Michell's rule). ε may or may not express the strain field in the basis in which it is diagonal. Actually, ε expresses the strain field in the predetermined curvilinear coordinate system we chose. What matters is only whether the tensor ε is such that it meets Michell's rule, which determines if it is acceptable or not. Hence, applying Michell's rule to ε, it follows that the eigenvalues of ε shall be equal in absolute value and opposed in sign, which forces the trace of ε to be zero-valued. Then ε becomes:

$$
\varepsilon = \begin{pmatrix} \varepsilon_\alpha & \varepsilon_{\alpha\beta} \\[3mm] \varepsilon_{\alpha\beta} & -\varepsilon_\alpha \end{pmatrix} \tag{3.10}
$$

With:

$$
\begin{cases} \varepsilon_\alpha = \dfrac{1}{A}\dfrac{\partial u_\alpha}{\partial \alpha} + \dfrac{1}{AB}\dfrac{\partial A}{\partial \beta}u_\beta \\[3mm] \qquad = -\left(\dfrac{1}{B}\dfrac{\partial u_\beta}{\partial \beta} + \dfrac{1}{AB}\dfrac{\partial B}{\partial \alpha}u_\alpha\right) \\[3mm] \varepsilon_{\alpha\beta} = \dfrac{1}{2}\left(\dfrac{B}{A}\dfrac{\partial}{\partial \alpha}\left(\dfrac{u_\beta}{B}\right) + \dfrac{A}{B}\dfrac{\partial}{\partial \beta}\left(\dfrac{u_\alpha}{A}\right)\right) \end{cases} \tag{3.11}
$$

Then, we solve the equation stating that eigenvalues ε_I and ε_II of $\boldsymbol{\varepsilon}$ shall be equal in absolute value to ε and opposed in sign. From equation 3.10 we find:

$$\begin{cases} \varepsilon_\mathrm{I} = \sqrt{\varepsilon_\alpha^2 + \varepsilon_{\alpha\beta}^2} \\ \varepsilon_\mathrm{II} = -\varepsilon_\mathrm{I} \end{cases} \tag{3.12}$$

Which makes us ultimately solving:

$$\varepsilon_\alpha^2 + \varepsilon_{\alpha\beta}^2 = \varepsilon \tag{3.13}$$

If a solution to the above equation is found, then $\boldsymbol{\varepsilon}$ is acceptable, as it meets Michell's rule. Eigenvectors $\boldsymbol{\pi}_\mathrm{I}$ and $\boldsymbol{\pi}_\mathrm{II}$ of $\boldsymbol{\varepsilon}$ are computed on every point within Ω, and the lines of the Michell structure are generated.

3.2.2   Hemp-Chan procedure

In Hemp-Chan procedure, the strain tensor $\boldsymbol{\varepsilon}$ must express the strain field in the basis in which $\boldsymbol{\varepsilon}$ is diagonal. Equation 3.13 is therefore not solved directly - whereas it is in MSTM.

Instead of directly solving equation 3.13, Hemp-Chan procedure consists in introducing the angle ϕ that $\boldsymbol{e_\alpha}$ shares with the fixed vector of the Cartesian coordinate system $\boldsymbol{e_x}$, so that the tensor $\boldsymbol{\varepsilon}$ is in its diagonal form:

$$\boldsymbol{\varepsilon} = \begin{pmatrix} \varepsilon & 0 \\ 0 & -\varepsilon \end{pmatrix} \tag{3.14}$$

In other words, ϕ is the rotation for the Cartesian basis vectors to become the diagonalizing basis of the strain tensor at point $\mathrm{M}(\alpha,\beta)$. From the definition of ϕ it follows that:

$$\begin{cases} \boldsymbol{e_\alpha} = \cos(\phi)\boldsymbol{e_x} + \sin(\phi)\boldsymbol{e_y} \\ \boldsymbol{e_\beta} = -\sin(\phi)\boldsymbol{e_x} + \cos(\phi)\boldsymbol{e_y} \end{cases} \tag{3.15}$$

Derivatives of $\boldsymbol{e_\alpha}$ are then:

$$\begin{cases} \dfrac{\partial \boldsymbol{e_\alpha}}{\partial \alpha} = \dfrac{\partial \phi}{\partial \alpha}\left(-\sin(\phi)\boldsymbol{e_x} + \cos(\phi)\boldsymbol{e_y}\right) \\[2mm] \qquad = \dfrac{\partial \phi}{\partial \alpha}\boldsymbol{e_\beta} \\[2mm] \dfrac{\partial \boldsymbol{e_\alpha}}{\partial \beta} = \dfrac{\partial \phi}{\partial \beta}\left(-\sin(\phi)\boldsymbol{e_x} + \cos(\phi)\boldsymbol{e_y}\right) \\[2mm] \qquad = \dfrac{\partial \phi}{\partial \beta}\boldsymbol{e_\beta} \end{cases} \tag{3.16}$$

Comparing equation 3.16 to 3.4, we find:

$$\begin{cases} \dfrac{\partial \phi}{\partial \alpha} = -\dfrac{1}{B}\dfrac{\partial A}{\partial \beta} \\[3mm] \dfrac{\partial \phi}{\partial \beta} = \dfrac{1}{A}\dfrac{\partial B}{\partial \alpha} \end{cases} \tag{3.17}$$

Which corresponds to equation 4.14 in Hemp [7] or 6 in Chan [18]. Then, the solution for ϕ can be found by equaling equations 3.9 and 3.14, while taking equation 3.17 into account. Result is:

$$\begin{cases} \dfrac{1}{A}\left(\dfrac{\partial u_\alpha}{\partial \alpha} - \dfrac{\partial \phi}{\partial \alpha}u_\beta\right) = \varepsilon \\[3mm] \dfrac{1}{B}\left(\dfrac{\partial u_\beta}{\partial \beta} + \dfrac{\partial \phi}{\partial \beta}u_\alpha\right) = -\varepsilon \\[3mm] \dfrac{1}{A}\left(\dfrac{\partial u_\beta}{\partial \alpha} + \dfrac{\partial \phi}{\partial \alpha}u_\alpha\right) + \dfrac{1}{B}\left(\dfrac{\partial u_\alpha}{\partial \beta} - \dfrac{\partial \phi}{\partial \beta}u_\beta\right) = 0 \end{cases} \tag{3.18}$$

Introducing the local rotation ω as defined in Love[25], equation 38, and used in Chan[18], will make the rest of the calculation more straightforward. This is the only reason why it is introduced, as there is no condition on ω. By definition, we have:

$$2\omega = \frac{1}{AB}\left(\frac{\partial B}{\partial \alpha}u_\beta - \frac{\partial A}{\partial \beta}u_\alpha\right) + \frac{1}{A}\frac{\partial u_\beta}{\partial \alpha} - \frac{1}{B}\frac{\partial u_\alpha}{\partial \beta} \tag{3.19}$$

Using equation 3.17, we find:

$$2\omega = \frac{1}{A}\left(\frac{\partial u_\beta}{\partial \alpha} + \frac{\partial \phi}{\partial \alpha}u_\alpha\right) - \frac{1}{B}\left(\frac{\partial u_\alpha}{\partial \beta} - \frac{\partial \phi}{\partial \beta}u_\beta\right) \tag{3.20}$$

Combining equations 3.18 and 3.20 returns:

$$\begin{cases} \dfrac{\partial u_\alpha}{\partial \alpha} = A\varepsilon + \dfrac{\partial \phi}{\partial \alpha} u_\beta \\[2mm] \dfrac{\partial u_\beta}{\partial \beta} = -B\varepsilon - \dfrac{\partial \phi}{\partial \beta} u_\alpha \\[2mm] \dfrac{\partial u_\alpha}{\partial \beta} = -B\omega + \dfrac{\partial \phi}{\partial \beta} u_\beta \\[2mm] \dfrac{\partial u_\beta}{\partial \alpha} = A\omega - \dfrac{\partial \phi}{\partial \alpha} u_\alpha \end{cases} \tag{3.21}$$

Following equation (9) in Chan[18], from equation 3.21 we find that ϕ shall verify:

$$\frac{\partial^2 \phi}{\partial \alpha \partial \beta} = 0 \tag{3.22}$$

3.2.3   Proof conclusion

The analysis of the Hemp-Chan procedure has shown that Michell structures were generated by finding the curvilinear basis at point M (α,β) in which the strain tensor $\boldsymbol{\varepsilon}$ is diagonal and follows Michell's rule. The aforementioned curvilinear basis is parametrized by the angle ϕ it has with the Cartesian basis. All these conditions lead to solving the equations shown in equation 3.18, which turns out to be equivalent to solving equation 3.22.

In MSTM, the curvilinear basis remains constant. The strain tensor $\boldsymbol{\varepsilon}$ is expressed in such basis and implemented to see if it can satisfy Michell's rule. If it does, eigenvectors of $\boldsymbol{\varepsilon}$ are computed and the Michell structure is generated. Therefore, the curvilinear basis at point M (α,β) in which the strain tensor $\boldsymbol{\varepsilon}$ is diagonal is found after ensuring that $\boldsymbol{\varepsilon}$ respects Michell's rule, and not at the same time as in Hemp-Chan procedure. Note that the diagonalizing $\boldsymbol{\varepsilon}$ is not about rotating the Cartesian basis anymore, but the curvilinear basis of reference.

By showing that the only true difference between Hemp-Chan procedure and MSTM is about when the diagonalization of $\boldsymbol{\varepsilon}$ is performed and what the affected basis is, we conclude that both methods are equivalent in 2D. Ultimately, both methods find the exact same basis in which $\boldsymbol{\varepsilon}$ is diagonal, and use its basis vectors to generate a

Michell structure.

Both methods are equivalent in 2D, but MSTM has advantages in 3D over the Hemp-Chan procedure. Indeed, the Hemp-Chan procedure for 3D would require the introduction of two other angles in equation 3.15, each referring to the rotation to perform around each of the three axes. This study will be mentioned in section 6.2 *Future work*. In contrast, MSTM can apply to 3D by using a 3×3 tensor matrix rather than a 2×2 one

3.3 MSTM algorithm

In this section, the algorithm corresponding to MSTM is defined. It is designed to draw lines which are part of a Michell strain field and works for either two or three dimensional cases. The functioning is as follows:

- Step 0: This step corresponds to the pre-initialization of the algorithm. We define a domain Ω, submitted to given loading and/or displacement conditions. We then determine what the expression of $\boldsymbol{\varepsilon}$ needs to be so as to (1) meet Michell's rule or Lewinsky's criteria and (2) meet the boundary conditions of the problem. More details about the procedure in this step are given in section 3.1. We also define a step value δ used in step 4.

- Step 1: We pick a set of starting points $\left(M_{0,i}\right)_{1 \leq i \leq K}$, preferably on a border of Ω.

- Step 2: We estimate $\boldsymbol{\varepsilon}$ for each $M_{0,i}$.

- Step 3: We diagonalize $\boldsymbol{\varepsilon}$ and determine $\boldsymbol{\pi_{1,i}}$ and $\boldsymbol{\pi_{2,i}}$ for each $M_{0,i}$, $\boldsymbol{\pi_{1,i}}$ and $\boldsymbol{\pi_{2,i}}$ corresponding to the respective maximal and minimal eigenvalue of $\boldsymbol{\varepsilon}$, $+\varepsilon$ and $-\varepsilon$, $\varepsilon > 0$.

- Step 4: We define $M_{1,i}$ and $M_{2,i}$ in order to have a first order graphical approx-

imation of the Michell structure:

$$\begin{cases} \boldsymbol{OM_{1,i}} = \boldsymbol{OM_{0,i}} + \delta\boldsymbol{\pi_{1,i}} \\ \boldsymbol{OM_{2,i}} = \boldsymbol{OM_{0,i}} + \delta\boldsymbol{\pi_{2,i}} \end{cases}$$

Where O is the origin of the coordinate system.

- Step 5: We draw members $[M_{0,i}M_{1,i}]$ and $[M_{0,i}M_{2,i}]$

- Step 6: We estimate $\boldsymbol{\varepsilon}$ for each $M_{1,i}$ and for each $M_{2,i}$.

- Step 7: We compute $\boldsymbol{\pi_{1,i}}$ for each $M_{1,i}$ and $\boldsymbol{\pi_{2,i}}$ for each $M_{2,i}$.

- Step 8: We define $M'_{1,i}$ and $M'_{2,i}$ as:

$$\begin{cases} \boldsymbol{OM'_{1,i}} = \boldsymbol{OM_{1,i}} + \delta\boldsymbol{\pi_{1,i}} \\ \boldsymbol{OM'_{2,i}} = \boldsymbol{OM_{2,i}} + \delta\boldsymbol{\pi_{2,i}} \end{cases}$$

- Step 9: We draw members $[M_{1,i}M'_{1,i}]$ and $[M_{2,i}M'_{2,i}]$

- Step 10: We assign the values $M'_{1,i}$ and $M'_{2,i}$ in $M_{1,i}$ and $M_{2,i}$ and go back to step 6 as long as $M_{1,i}$ and $M_{2,i}$ are within Ω.
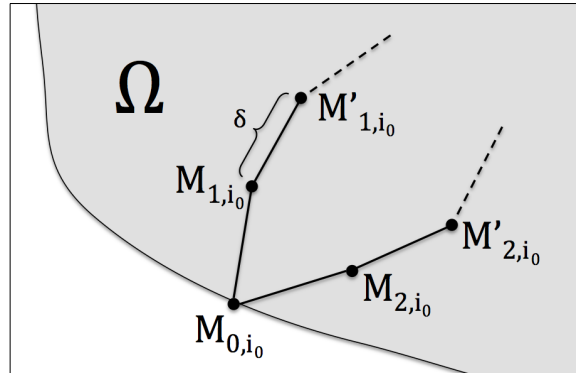
Figure 3-1: Functioning of the tensor-based algorithm.

Figure 3-1 illustrates the typical functioning of the algorithm for a given i. Steps 6 to 10 make the complexity of the algorithm equal to $\mathcal{O}(1)$, which is the maximal speed possible. Had the algorithm initiate its loop at the end of step 5, its complexity would be $\mathcal{O}(2^N)$ - as it generates two points out of one at each loop iteration.

The algorithm hence generates the lines of tension or compression starting at $\left(M_{0,i}\right)_{1\leq i\leq K}$ and reaching a boundary of Ω. As optimum structures typically consist in an infinite amount of tension and compression lines, the algorithm only generates sub-sets of such optimum structures. Its true advantage consists in its speed, when compared with other algorithms for numerical structural optimization.

We actually believe that it is of utmost importance to physically understand the output of an optimization algorithm. The rather simple algorithm here shows lines of principal strains that follow an analytical analysis of the problem, which makes the user fully aware of what is going on. We believe that such an approach adds value to the solution: we can understand why the Michell structure found by the algorithm looks the way it looks, because we know what the underlying equations are. We can hence answer questions beyond just what the solution looks like: Why does the solution look this way? How does it work? What is the equation of the volume of the solution?, etc.

THIS PAGE INTENTIONALLY LEFT BLANK

Chapter 4

Results in 2D

4.1 Case study: Michell wheel

4.1.1 Problem statement

Let Ω be the region of plane between two concentric circles of radii R_1 and R_2, with $R_1 < R_2$. Because of the domain geometry, we use a polar coordinate system (r,θ) which origin O is the center of the two aforementioned circles. The circle of radius R_1 is fixed, hence experiences no displacement. The circle of radius R_2 experiences the orthoradial displacement $U\boldsymbol{e_\theta}$.

Boundary conditions are hence:

$$\begin{cases} \boldsymbol{u}(r = R_1) = \boldsymbol{0} \\ \boldsymbol{u}(r = R_2) = U\boldsymbol{e_\theta} \end{cases} \tag{4.1}$$

Because the problem is invariant by rotation, we derive that the displacement $\boldsymbol{u}$ in any point within Ω is such that:

$$\boldsymbol{u}(r, \theta) = u_\theta(r)\boldsymbol{e_\theta} \tag{4.2}$$
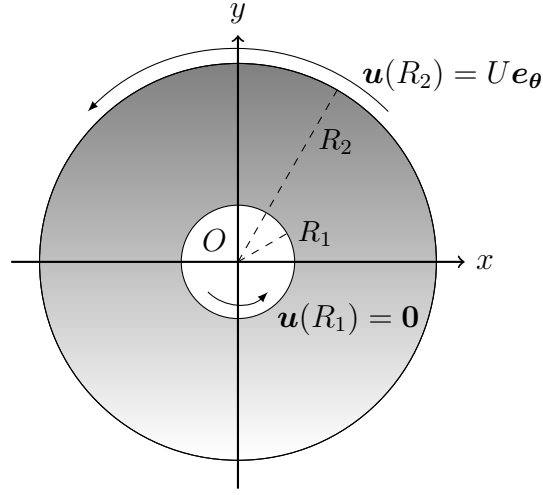
Figure 4-1: Michell wheel problem statement.

4.1.2 Finding the strain tensor

By equations 3.1, 4.2 and Sadd equation (2.7.3),the general strain field equation is:

$$\boldsymbol{\varepsilon}(r) = \frac{1}{2}\left(\boldsymbol{\nabla u} + \boldsymbol{\nabla u^\mathsf{T}}\right) = e_{r\theta}\boldsymbol{m_{r\theta}} \tag{4.3}$$

With:

$$\boldsymbol{m_{r\theta}} = \begin{pmatrix} 0 & 1 \\ 1 & 0 \end{pmatrix} \tag{4.4}$$

And:

$$e_{r\theta} = \frac{1}{2}\left(\frac{\mathrm{d}u_\theta}{\mathrm{d}r} - \frac{u_\theta}{r}\right) \tag{4.5}$$

Equation 4.3 gives the following principal strains ε_I and ε_II:

$$\begin{cases} \varepsilon_\mathrm{I} = e_{r\theta} \\ \varepsilon_\mathrm{II} = -\varepsilon_\mathrm{I} \end{cases} \tag{4.6}$$

Following Michell's rule, let's solve $\varepsilon_\mathrm{I} = \varepsilon$, with ε a given constant strain. Using equations 4.6 and 4.5 we find:

$$\frac{\mathrm{d}u_\theta}{\mathrm{d}r} - \frac{u_\theta}{r} = 2\varepsilon \tag{4.7}$$

Solution for the above differential equation meeting the first boundary condition in equation 4.1 is:

$$u_\theta(r) = 2\varepsilon r \ln\left(\frac{r}{R_1}\right) \tag{4.8}$$

This equation is equivalent to Hemp, equation (4.85), found for the same case study. This helps to validate the strain tensor approach we have developed.

A relation between U and ε appears in order to satisfy the second boundary condition in equation 4.1:

$$\frac{U}{\varepsilon} = 2R_2 \ln\left(\frac{R_2}{R_1}\right) \tag{4.9}$$

From equation 4.3 eigenvectors $\boldsymbol{\pi}_{\mathrm{I}}$ and $\boldsymbol{\pi}_{\mathrm{II}}$ verify:

$$\begin{cases} \boldsymbol{\pi}_{\mathrm{I}} \parallel \boldsymbol{e_r} + \boldsymbol{e_\theta} \\ \boldsymbol{\pi}_{\mathrm{II}} \parallel \boldsymbol{e_r} - \boldsymbol{e_\theta} \end{cases} \tag{4.10}$$

Which means:

$$\begin{cases} \overrightarrow{(\boldsymbol{e_r}, \boldsymbol{\pi}_{\mathrm{I}})} = \dfrac{\pi}{4} \\ \overrightarrow{(\boldsymbol{e_r}, \boldsymbol{\pi}_{\mathrm{II}})} = -\dfrac{\pi}{4} \end{cases} \tag{4.11}$$

The geometry we expect our algorithm to return is hence one with intersections at
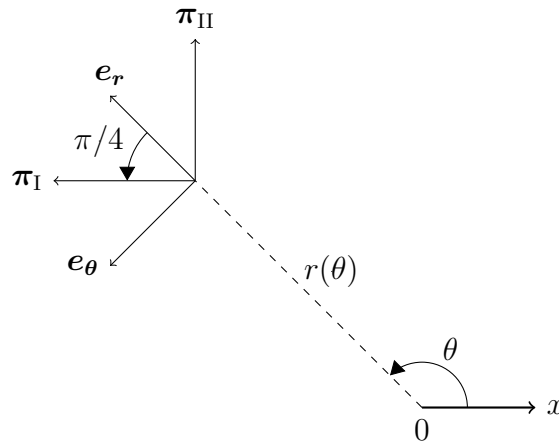
Figure 4-2: Geometrical relations for Michell wheel.

right angles and rotated by $\frac{\pi}{4}$ from $\boldsymbol{e_r}$ - see figure 4-2. Such geometrical relations were also found in Hemp, figure (4.11), reproduced in figure 4-3. This problem and
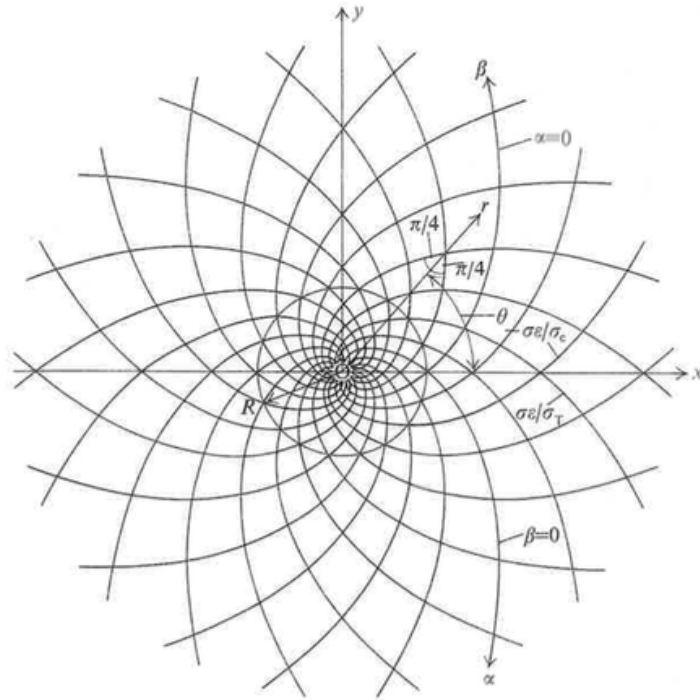
Figure 4-3: Michell wheel, as shown in Hemp[7].

result are called the Michell wheel.

4.1.3   Parametric generations based on MSTM

The results obtained from this algorithm correspond to the expectations from the previous subsection. They are shown in figure 4-4.
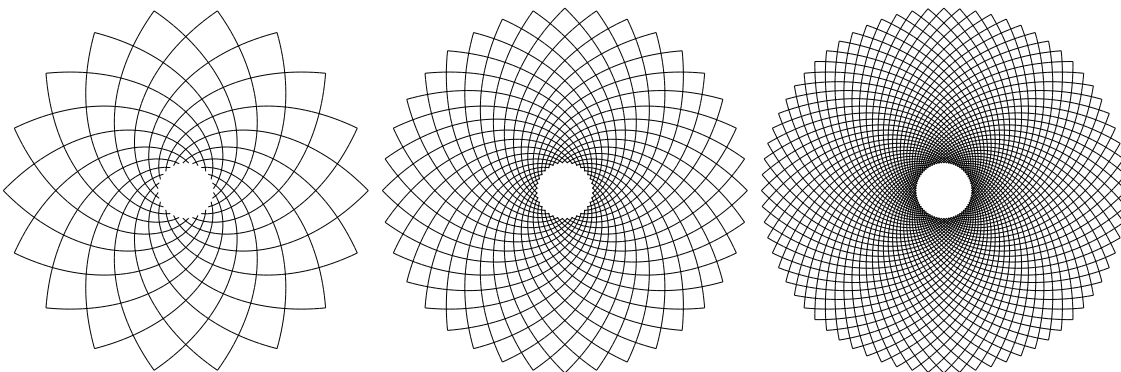
Figure 4-4: Algorithm output - 18, 36 and 72 starting points.

4.1.4   Equation of the Michell wheel lines

Let us find what typical equation the lines of compression or tension within the structure have. From equation 4.11 and figure 4-2, we derive that:

$$r\frac{\mathrm{d}\theta}{\mathrm{d}r} = \tan\left(\pm\frac{\pi}{4}\right) = \pm 1 \tag{4.12}$$

Which leads to:

$$r(\theta) = \pm R_1 e^{(\theta-\theta_0)} \tag{4.13}$$

We found such equation by adding the condition $r(\theta_0) = R_1$. Again, the same lines equation is found in Hemp[7], equation (4.82).

4.1.5   Volume of Michell wheel

With equations 4.6 and 4.7, we have built a strain field in which axial strain is the same in absolute value whatever the member. For a circular orthoradial load f_θ distributed on $r = R_2$ that induces the orthoradial displacement U, the external work W is:

$$W = \int_{\theta=0}^{2\pi} f_\theta U R_2 \,\mathrm{d}\theta$$
$$= 2\pi f_\theta U R_2 \tag{4.14}$$

The reaction moments on $r = R_1$ do not imply any displacement; its work is therefore equal to zero. We can then use Michell's second theorem by replacing the sign of inequality by that of equality in equation 2.19. We consider the maximum stress capacity be the same in either tension or compression and equal to σ. The minimal volume V_m is hence:

$$\sigma V_m = \frac{W}{\varepsilon} \tag{4.15}$$

Taking equations 4.9 and 4.15 into account, we find:

$$V_m = \frac{4\pi}{\sigma} f_\theta R_2^2 \ln\left(\frac{R_2}{R_1}\right) \tag{4.16}$$

By defining the external torque T such that:

$$T = \int_{\theta=0}^{2\pi} f_\theta R_2^2 \, \mathrm{d}\theta = 2\pi f_\theta R_2^2 \tag{4.17}$$

The volume of the Michell structure becomes:

$$V_m = \frac{2T}{\sigma} \ln\left(\frac{R_2}{R_1}\right) \tag{4.18}$$

There has not been a calculation of the volume of Michell wheel presented in the literature prior to the results shown here, but the above is consistent with the calculation for Michell cantilever shown in the end of next section, *Case study: Michell cantilever*.

4.2   Case study: Michell cantilever

4.2.1   Problem statement

We keep the same problem as for the Michell wheel, but set the number of nodes at the external boundary of Ω to 1. This is the starting point for the algorithm. We therefore only consider the substructure that resists a local orthoradial loading $\boldsymbol{F_\theta}$ (and displacement $U\boldsymbol{e_\theta}$) located at $r = R_2$ - see figure 4-5 below.

4.2.2   Volume of Michell cantilever

Applying what we found in section 4.1.5 *Volume of Michell wheel* to the cantilever loading condition described in section 4.2.1, the minimal volume V_m is such that:

$$\sigma V_m = F_\theta \frac{U}{\varepsilon} \tag{4.19}$$
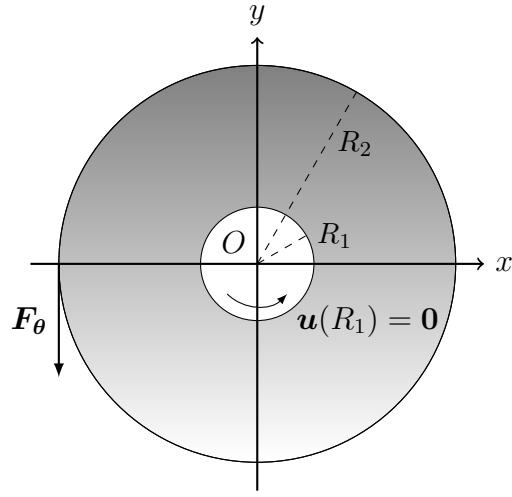
Figure 4-5: Michell cantilever problem statement.

Taking equation 4.9 into account, we find:

$$V_m = \frac{2}{\sigma} F_\theta R_2 \ln\left(\frac{R_2}{R_1}\right) \tag{4.20}$$

This equation is identical to Hemp[7], equation (4.93) and Michell for equal maximal tension and compression stress capacities - i.e. $f_t = f_c = \sigma$.

4.2.3 Parametric generations based on MSTM

Results from the algorithm are shown in figure 4-7. Such shapes correspond to what Michell himself finds for the same problem - see figure 4-6, taken from his publication[1].
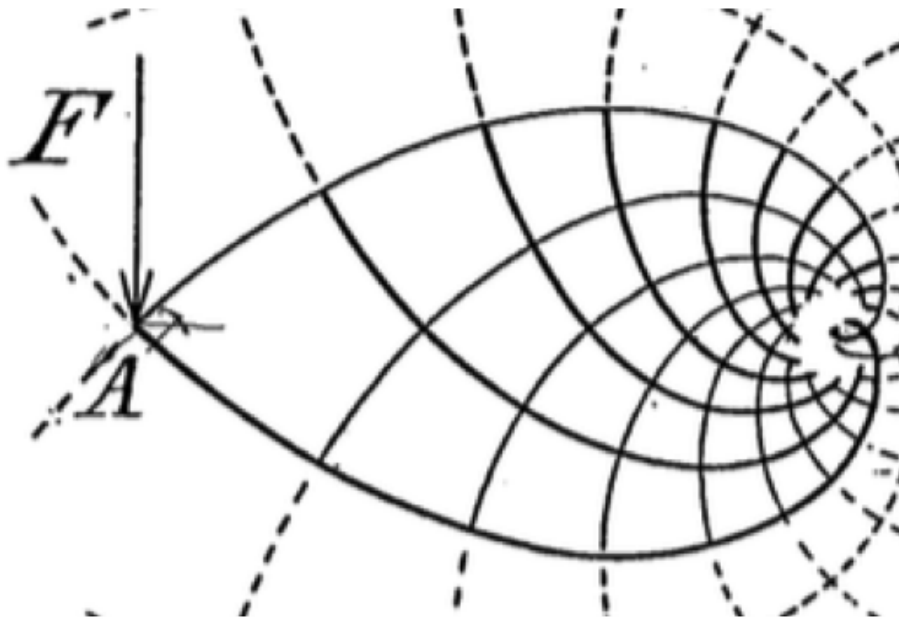
Figure 4-6: original Michell cantilever, as found in Michell[1].
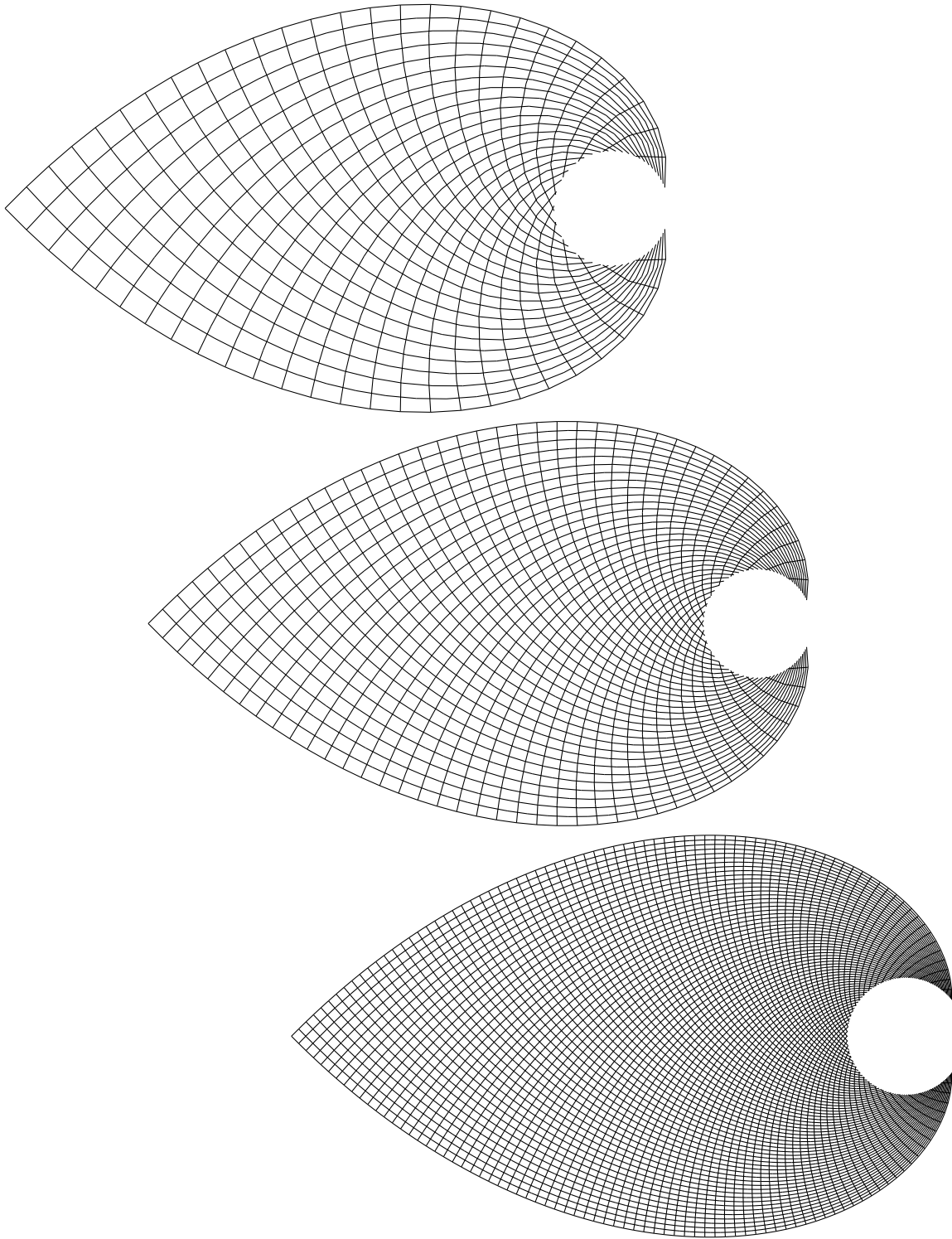
Figure 4-7: Cantilever solution found with the algorithm for decreasing values of the step parameter δ.

THIS PAGE INTENTIONALLY LEFT BLANK

Chapter 5

Results in 3D

In this chapter, we will use spherical coordinates. We hence define the spherical coordinates (r,φ,θ) as shown in figure 5-1. It follows that: $r \in \mathbb{R}^+, \theta \in [0, 2\pi], \varphi \in [0, \pi]$. θ is the radial angle, φ is the colatitude angle. Any general formula for this coordinate system can be found in Sadd[24], appendix A.
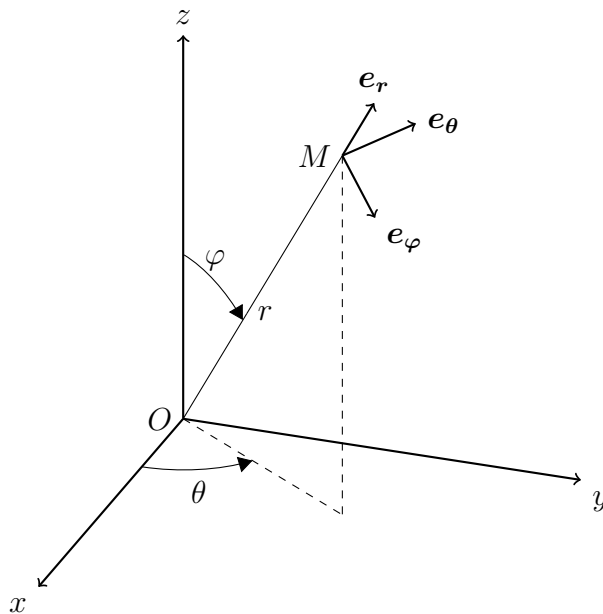
Figure 5-1: Definition of the spherical coordinates system.

5.1 Implementation of MSTM algorithm

In this section, let us develop what the shift from two to three dimensions implies for the strain tensor based algorithm introduced in section 3.3 *MSTM algorithm.*

5.1.1 Pre-initialization

We will keep analyzing any problem by first finding the general expression of the displacement $\boldsymbol{u}(r, \varphi, \theta)$. Based on the problem geometry, we will select the relevant variables amid r, φ, θ and basis vectors amid $\boldsymbol{e_r}, \boldsymbol{e_\varphi}, \boldsymbol{e_\theta}$. Even though variables and basis vectors differ from the ones in chapter 4 *Results in 2D*, the procedure remains essentially the same.

Then, we will find what the corresponding expression of the strain tensor $\boldsymbol{\varepsilon}$ is, following equation 3.1.

Finally, the analytical expression for both $\boldsymbol{u}(r, \varphi, \theta)$ and $\boldsymbol{\varepsilon}$ will be found after forcing the maximal and minimal eigenvalues of $\boldsymbol{\varepsilon}$ to be constant, opposed and equal in absolute value. We hence apply Lewinsky's criteria for three dimensional Michell structures, as introduced in section 2.4.2 *A criteria for 3D Michell structures.*

5.1.2 Diagonalization of the strain tensor

As shown in appendices C, D and E, we introduce the function "TriDimLewinskyEigen" in the algorithm. It will be called out each time eigenvectors $\boldsymbol{\pi_M}$ and $\boldsymbol{\pi_m}$ of $\boldsymbol{\varepsilon}$ need to be computed. This function returns such vectors, so that $\boldsymbol{\pi_M}$ corresponds to the maximal eigenvalue of $\boldsymbol{\varepsilon}$ and $\boldsymbol{\pi_m}$ to its minimal eigenvalue. The corresponding code is shown in figure 5-2.

```
function [Pi_M,Pi_m]=TriDimLewinskiEigen(M)
    [V,D]=eig(M);
    lambda_M=D(1,1);lambda_m=D(1,1);
    Pi_M=V(:,1);Pi_m=V(:,1);
    for i=2:1:3
        if D(i,i)>lambda_M
            lambda_M=D(i,i);
            Pi_M=V(:,i);
        end
        if D(i,i)<lambda_m
            lambda_m=D(i,i);
            Pi_m=V(:,i);
        end
    end
end
```

Figure 5-2: An additive function to the strain tensor algorithm for 3D cases.

5.2   Case study: Michell sphere

5.2.1   Problem statement

We consider two coaxial discs of respective radii R_1 and R_2, in $\Omega = \mathbb{R}^3$. The discs are perpendicular to their shared axis, z. Each rotates around z with respective rotations ω_1 and ω_2, which can be induced by torques for example. This problem can therefore be seen as a transmission of torques.

The origin of the coordinate system, O, is such that it is on the z axis at an equal distance R from both of the disc perimeters. The existence of such position whatever the value of R_1 and R_2 can be proved through straightforward trigonometry. As a consequence, O may not be in between the two discs.

Because both the geometry and the motion conditions of the problem are invariant with respects to θ, θ will not be a variable for any function describing the problem. $\boldsymbol{u}$ is therefore a function of r and φ only. Also, displacements on the discs being orthoradial only, we assume $\boldsymbol{u}$ is orthoradial anywhere within Ω.

We actually can make as many assumptions as we want on $\boldsymbol{u}$: if they lead to a strain

field that meets Lewinsky's criteria, the assumptions will be validated. Otherwise, they will have to be re-evaluated. We assume the rotation ω within Ω does not vary
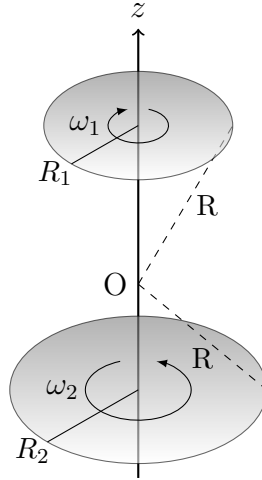
Figure 5-3: Problem statement of Michell sphere.

with r. Put differently, we see Ω as being an infinite superimposition of cones which summits are in O. Each cone rotates at its own pace $\omega(\varphi)$. We end up finding the following expression for $\boldsymbol{u}$:

$$\boldsymbol{u} = r\sin(\varphi)\omega(\varphi)\boldsymbol{e_\theta} \tag{5.1}$$

It will prove useful to also introduce the colatitudes φ_1 and φ_2 of the two discs, such that:

$$\begin{cases} R\sin(\varphi_1) = R_1 \\ R\sin(\varphi_2) = R_2 \end{cases} \tag{5.2}$$

Taking equations 5.1 and 5.2 into account, boundary conditions on $\boldsymbol{u}$ are:

$$\begin{cases} R\sin(\varphi_1)\omega(\varphi_1) = R_1\omega_1 \\ R\sin(\varphi_2)\omega(\varphi_2) = R_2\omega_2 \end{cases} \tag{5.3}$$

Or, after simplification:

$$\begin{cases} \omega(\varphi_1) = \omega_1 \\ \omega(\varphi_2) = \omega_2 \end{cases} \tag{5.4}$$

Again, equation 5.1 is an assumption at this stage of the calculation. It has been found by trying to adapt $\boldsymbol{u}$ to the given problem geometry. Boundary conditions

have then been adapted to equation 5.1. In any case, the assumed expression for $\boldsymbol{u}$ will be validated if it leads to an acceptable strain tensor, i.e. if Lewinsky's criteria is met.

5.2.2 Finding the strain tensor

We use equation 5.1 in equation 3.1 and find, per Sadd, chapter 2, equation (2.7.5):

$$\boldsymbol{\varepsilon} = \varepsilon_{\varphi\theta}(\varphi)\boldsymbol{M_{\varphi\theta}} \tag{5.5}$$

Where:

$$\varepsilon_{\varphi\theta}(\varphi) = \frac{\sin(\varphi)}{2}\frac{\mathrm{d}\omega}{\mathrm{d}\varphi} \tag{5.6}$$

And $\boldsymbol{M_{\varphi\theta}}$ is defined as:

$$\boldsymbol{M_{\varphi\theta}} = \begin{pmatrix} 0 & 0 & 0 \\ 0 & 0 & 1 \\ 0 & 1 & 0 \end{pmatrix} \tag{5.7}$$

For the strain tensor found in equation 5.5 to be admissible with respects to Lewinsky's criteria, its maximum and minimum eigenvalues ε_{I} and $\varepsilon_{\mathrm{III}}$ need to be constantly equal to ε in absolute value, where ε is a parameter. From equation 5.5, maximal and minimal eigenvalues of the strain tensor ε_{I} and $\varepsilon_{\mathrm{III}}$ are:

$$\begin{cases} \varepsilon_{\mathrm{I}} = \varepsilon_{\varphi\theta}(\varphi) \\ \varepsilon_{\mathrm{III}} = -\varepsilon_I \end{cases} \tag{5.8}$$

Therefore $\varepsilon_{\mathrm{I}} = \varepsilon$ brings:

$$\sin(\varphi)\frac{\mathrm{d}\omega}{\mathrm{d}\varphi} = 2\varepsilon \tag{5.9}$$

Solutions for equation 5.9 exist for $\varphi \in]0, \pi[$. Integrating equation 5.9 between φ_1 and φ gives:

$$\omega(\varphi) - \omega(\varphi_1) = 2\varepsilon\left[\ln\left(\tan\left(\frac{\varphi}{2}\right)\right) - \ln\left(\tan\left(\frac{\varphi_1}{2}\right)\right)\right] \tag{5.10}$$

Taking the first boundary condition in equation 5.4, we have:

$$\omega(\varphi) = 2\varepsilon \left[\ln\left(\tan\left(\frac{\varphi}{2}\right)\right) - \ln\left(\tan\left(\frac{\varphi_1}{2}\right)\right) \right] + \omega_1 \tag{5.11}$$

In order to satisfy the second boundary condition in equation 5.4, a condition on the parameter ε arises (mathematically true for $\varphi_1 \neq \varphi_2$, which is always the case):

$$\varepsilon = \frac{\omega_2 - \omega_1}{2} \left[\ln\left(\tan\left(\frac{\varphi_2}{2}\right)\right) - \ln\left(\tan\left(\frac{\varphi_1}{2}\right)\right) \right]^{-1} \tag{5.12}$$

Which gives:

$$\omega(\varphi) = (\omega_2 - \omega_1)\frac{\ln\left(\tan\left(\frac{\varphi}{2}\right)\right) - \ln\left(\tan\left(\frac{\varphi_1}{2}\right)\right)}{\ln\left(\tan\left(\frac{\varphi_2}{2}\right)\right) - \ln\left(\tan\left(\frac{\varphi_1}{2}\right)\right)} + \omega_1 \tag{5.13}$$

We have been able to find a solution that meets both Lewinsky's criteria (equation 5.9) and the boundary conditions (equations 5.11 and 5.12), we have therefore found a Michell structure for the problem. Displacement $\boldsymbol{u}$ and strain tensor $\boldsymbol{\varepsilon}$ are then:

$$\boldsymbol{u} = r\sin(\varphi) \left[(\omega_2 - \omega_1)\frac{\ln\left(\tan\left(\frac{\varphi}{2}\right)\right) - \ln\left(\tan\left(\frac{\varphi_1}{2}\right)\right)}{\ln\left(\tan\left(\frac{\varphi_2}{2}\right)\right) - \ln\left(\tan\left(\frac{\varphi_1}{2}\right)\right)} + \omega_1 \right] \boldsymbol{e_\theta} \tag{5.14}$$

$$\boldsymbol{\varepsilon} = \frac{\omega_2 - \omega_1}{2} \left[\ln\left(\tan\left(\frac{\varphi_2}{2}\right)\right) - \ln\left(\tan\left(\frac{\varphi_1}{2}\right)\right) \right]^{-1} \boldsymbol{M_{\varphi\theta}} \tag{5.15}$$

5.2.3 MSTM parametric generation

The two maximum and minimum eigenvectors $\boldsymbol{\pi}_{\text{I}}$ and $\boldsymbol{\pi}_{\text{III}}$ found from equation 5.15 have the following directions:

$$\begin{cases} \boldsymbol{\pi}_{\text{I}} \parallel \boldsymbol{e_\theta} + \boldsymbol{e_\varphi} \\ \boldsymbol{\pi}_{\text{III}} \parallel \boldsymbol{e_\theta} - \boldsymbol{e_\varphi} \end{cases} \tag{5.16}$$

Using the Matlab code described in section 3.3 *MSTM algorithm*, and available in appendix C *Matlab code for Michell sphere*, we can generate solutions with increased accuracy by adding more and more lines - keeping all other parameters R, R_1 and R_2 equal. Adding lines makes the structure found by the algorithm closer and closer to the exact Michell solution, which has an infinity of lines. Such a generation is shown in figure 5-11a. We then make parameters R_1 and R_2 vary in figure 5-11b. Finally, we vary R in figure 5-5.
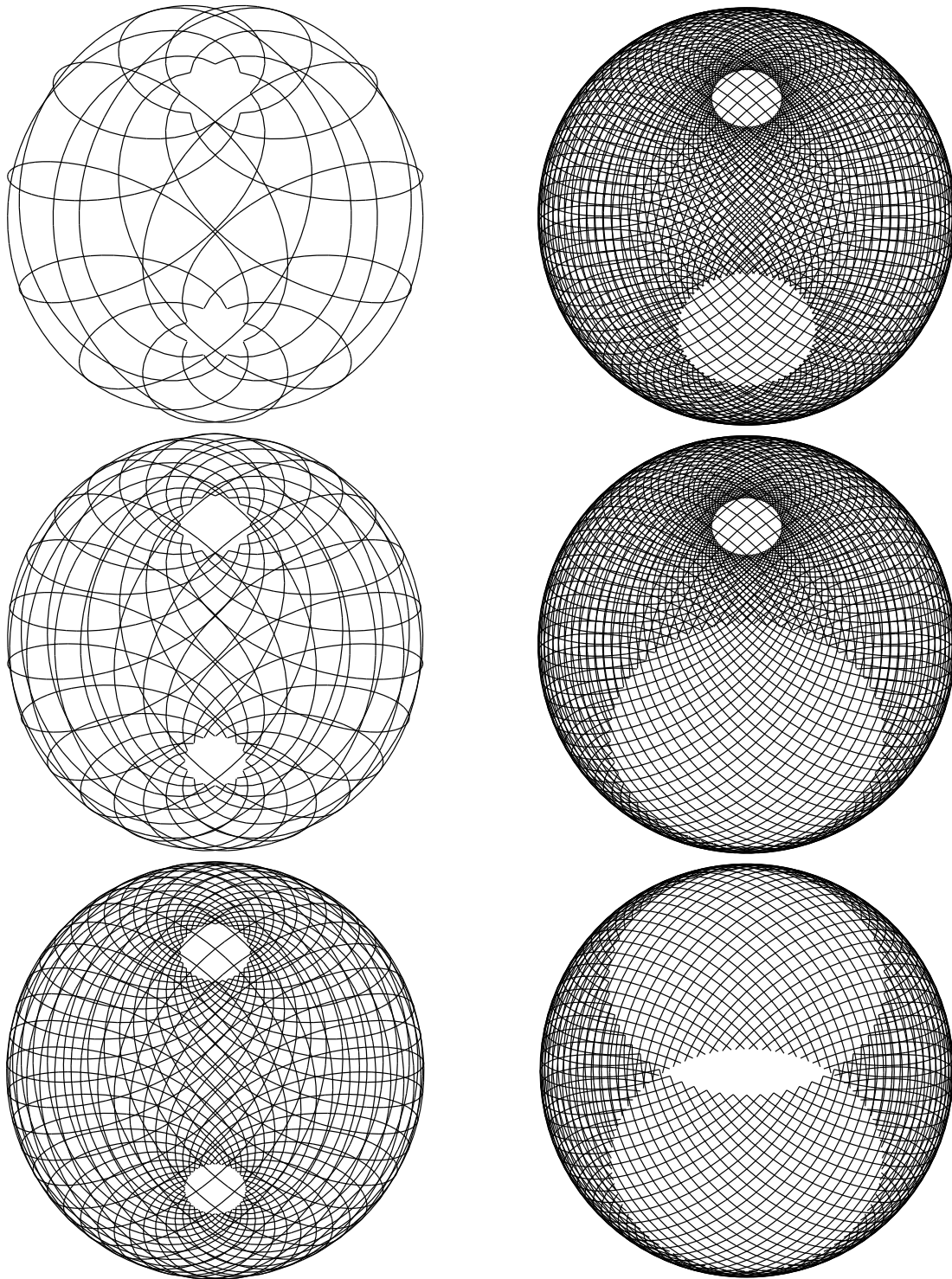
(a) 8, 16 and 32 starting points.

(b) Different disc radii R_1 and R_2.

Figure 5-4: Parametrized solutions.
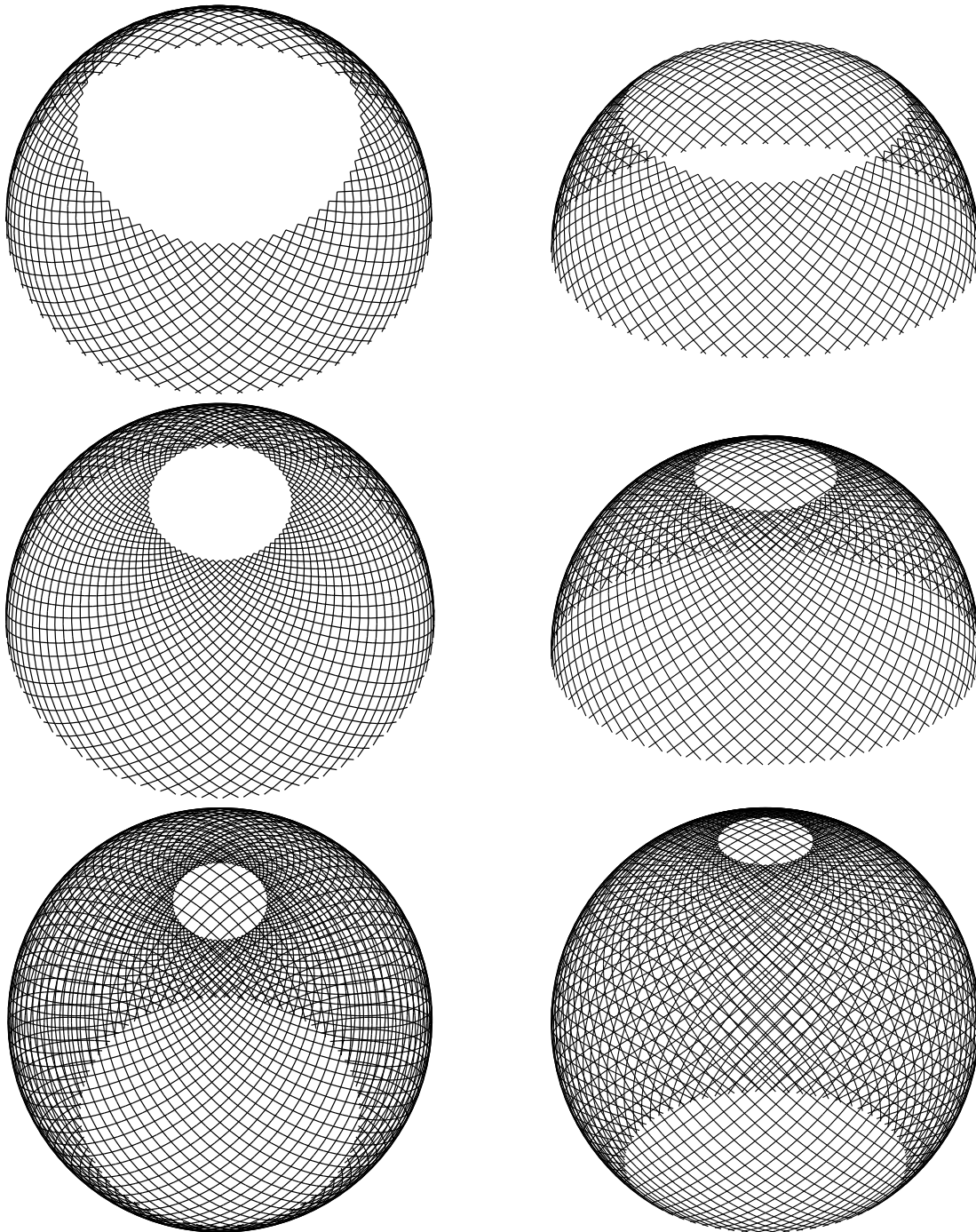
Figure 5-5: Solution for three different values of R: $\frac{R_2}{2}$ (top), R_2 (middle) and $3\frac{R_2}{2}$ (bottom).

5.2.4   Equation of the Michell sphere lines

An infinitely small displacement is expressed in spherical coordinates as:

$$\mathrm{d}\boldsymbol{OM} = \mathrm{d}r\boldsymbol{e_r} + r\sin(\varphi)\,\mathrm{d}\theta\boldsymbol{e_\theta} + r\,\mathrm{d}\varphi\boldsymbol{e_\varphi} \tag{5.17}$$

As we also have to verify that $\mathrm{d}\boldsymbol{OM} \parallel \boldsymbol{\pi_I}$ or $\boldsymbol{\pi_{III}}$, we can infer that, following equation 5.16:

$$\begin{cases} \mathrm{d}r = 0 \\ r\sin(\varphi)\,\mathrm{d}\theta = \pm r\,\mathrm{d}\varphi \end{cases} \tag{5.18}$$

Finding $\mathrm{d}r = 0$ explicitly shows that the lines of the structure will remain on a same sphere. It is a surface, or shell. In order to find the equation of such lines, we need to solve the second equation in 5.18. In other words, let's solve:

$$\frac{\mathrm{d}\theta}{\mathrm{d}\varphi} = \pm\frac{1}{\sin(\varphi)} \tag{5.19}$$

We see that the right-hand side of 5.19 is only defined for $\varphi \in]0, \pi[$. Integrating 5.19 between $\varphi_0 > 0$ and $\varphi < \pi$ gives:

$$\theta(\varphi) - \theta(\varphi_0) = \pm\left[\ln\left(\tan\left(\frac{\varphi}{2}\right)\right) - \ln\left(\tan\left(\frac{\varphi_0}{2}\right)\right)\right] \tag{5.20}$$

$$\begin{cases} \theta(\varphi) = \pm\ln\left(\tan\left(\frac{\varphi}{2}\right)\right) + \theta_0 \\ \theta_0 = \theta(\varphi_0) \pm \ln\left(\tan\left(\frac{\varphi_0}{2}\right)\right) \end{cases} \tag{5.21}$$

We have hence been able to find the typical equation of a line part of the torque-resisting structure. This equation perfectly describes the rhumb lines mentioned in Michell[1]. Hence, the tensor method can generate the exact same solution as Michell for 3D cases too.

On the poles ($\varphi = 0, \varphi = \pi$), the structure degenerates:

$$\lim_{\varphi \to 0^+} |\theta(\varphi)| = \lim_{\varphi \to \pi^-} |\theta(\varphi)| = +\infty \qquad (5.22)$$

Such divergence explains why torques can't be defined as being concentrated at the poles. Indeed, the closer φ gets to 0 or π, the "faster" θ will rotate along the z axis, its "speed" being defined by equation 5.19. The tensor method is actually not able to solve this limiting case, as input parameters shall be continuous and differentiable enough for the strain tensor to be defined as in equation 3.1. The case $\varphi_0 = 0$ shall be investigated, as emphasized in section 6.2 *Future work*. Here, the Michell structure can be found as long as $0 < \varphi_0 << 1$. It will return close-to-infinitely long lines. This is a good illustration that infinity and optimality are sometimes much conceptually closer than what intuition makes us think.

For a given φ_0, and $\theta_{i,0} = i\theta_0$ with $i \in \mathbb{N}$ so that $\theta_{i,0} \in [0, 2\pi]$, let's plot the lines defined by $\theta_i(\varphi) = \ln\left(\tan\left(\frac{\varphi}{2}\right)\right) + \theta_{i,0}$ and $\theta_i(\varphi) = -\ln\left(\tan\left(\frac{\varphi}{2}\right)\right) + \theta_{i,0}$ (Figure 5-6) and combine them (Figure 5-7).
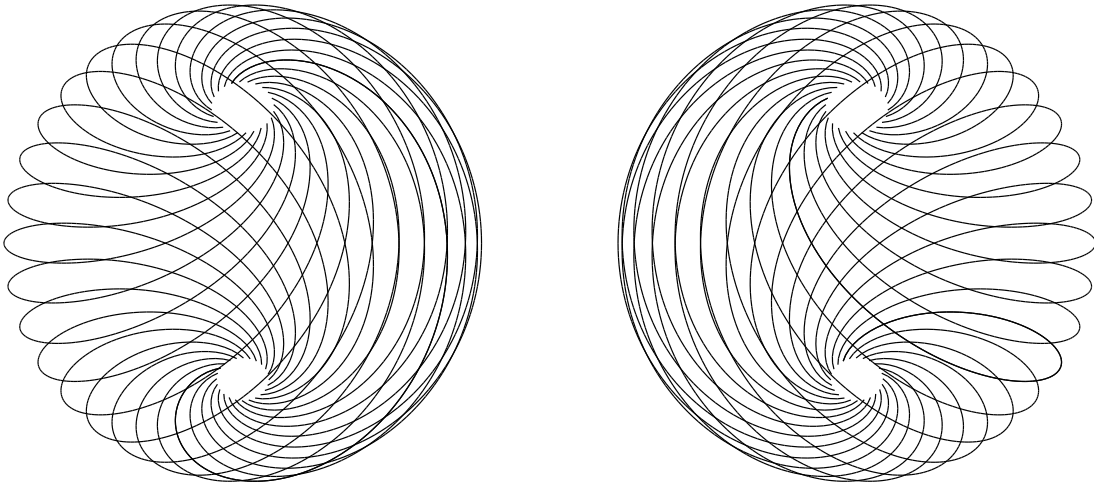
Figure 5-6: The two sets of lines from equation 5.21 - compression or tension.
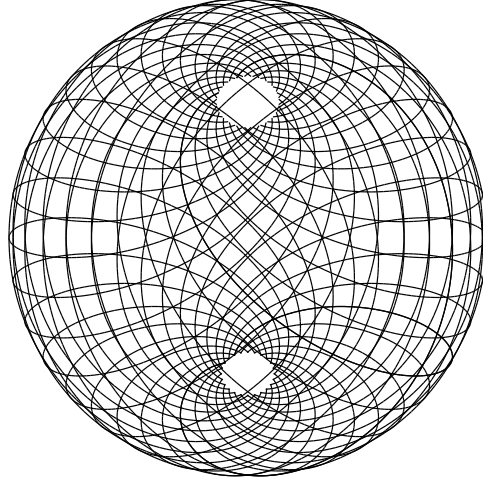
Figure 5-7: Combination of compression and tension: the Michell sphere.

5.2.5 Volume of Michell sphere

As described in 5.2.1 *Problem statement*, we consider the motion of the two discs to be caused by torques. More precisely, two distributed orthoradial loads $p_{1,\theta}$ and $p_{2,\theta}$ are applied on the perimeters of discs of respective radius R_1 and R_2.

External moment equilibrium is met for:

$$\int_{\theta=0}^{2\pi} p_{1,\theta} R_1^2 \, \mathrm{d}\theta + \int_{\theta=0}^{2\pi} p_{2,\theta} R_2^2 \, \mathrm{d}\theta = 0 \tag{5.23}$$

Which brings the equilibrium condition:

$$p_{1,\theta} R_1^2 = -p_{2,\theta} R_2^2 \tag{5.24}$$

The work of external forces W is:

$$W = \int_{\theta=0}^{2\pi} \left(p_{1,\theta} \omega_1 R_1^2 + p_{2,\theta} \omega_2 R_2^2 \right) \mathrm{d}\theta \tag{5.25}$$

Taking equation 5.24 into account, we find:

$$W = 2\pi p_{2,\theta} R_2^2 (\omega_2 - \omega_1) \tag{5.26}$$
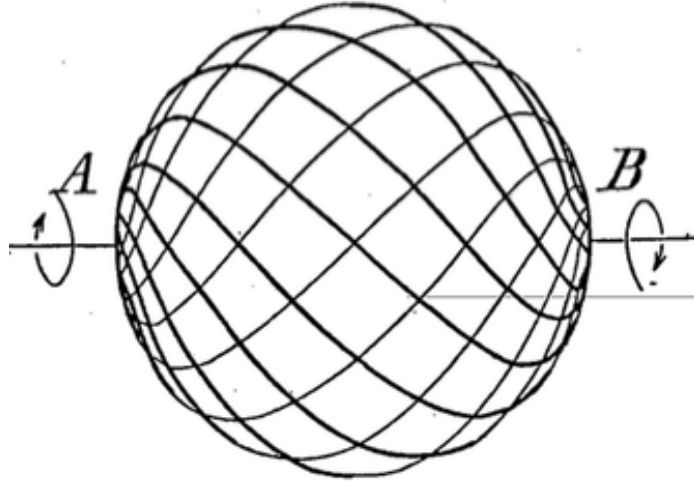
Figure 5-8: The original Michell sphere, as shown in Michell[1].

Applying equations 5.26 and 5.15 in equation 3.1, we can compute the minimal volume V_m of the Michell sphere:

$$V_m = \frac{4\pi p_{2,\theta} R_2^2}{\sigma} \left[\ln\left(\tan\left(\frac{\varphi_2}{2} \right) \right) - \ln\left(\tan\left(\frac{\varphi_1}{2} \right) \right) \right] \tag{5.27}$$

Let's notice that the simple case:

$$\begin{cases} R_1 = R_2 = R \\ \omega_2 = -\omega_1 = \omega \\ p_{2,\theta} = -p_{1,\theta} = p_\theta \\ \varphi_2 = \pi - \varphi_1 \end{cases} \tag{5.28}$$

This case has been studied in Michell[1], as shown in figure 5-8. Equation 5.28 reduces equation 5.27 to:

$$V_m = \frac{8\pi p_\theta R^2}{\sigma} \ln\left(\cot\left(\frac{\varphi}{2} \right) \right) \tag{5.29}$$

Introducing the torque T applied on discs, we have:

$$
\begin{aligned}
T &= \int_{\theta=0}^{2\pi} p_\theta R^2 \, \mathrm{d}\theta \\
&= 2\pi p_\theta R^2
\end{aligned}
\tag{5.30}
$$

And equation 5.29 becomes:

$$
V_m = \frac{4T}{\sigma} \ln\left(\cot\left(\frac{\varphi}{2}\right)\right)
\tag{5.31}
$$

This equation is identical to Hemp[7], equation (4.100) and Lewinski[27], equation (77) for the same case. Lewinski[27] also explains why the equation of the volume in Michell[1] is not exactly the same for this case.

The advantage of MSTM in this case study is that it enables us to find a broader range of solutions, because it allows radii R_1 and R_2 to be different.

5.3   Case study: 3D Michell cantilever

5.3.1   Problem statement

The spherical structure found in the above section 5.2 *Case study: Michell sphere* can be seen as being the superimposition of multiple substructures - just as in how section 4.2 *Case study: Michell cantilever* relates to section 4.1 *Case study: Michell wheel*. Each substructure is connected to an elementary orthoradial load $\boldsymbol{F_\theta}$ located on the perimeter of the disc of radius R_1 and is supported on the disc of radius R_2.

For external equilibrium to be verified, $\boldsymbol{F_\theta}$ induces moment reactions in the three directions of space on the disc of radius R_2. However, we consider the support as fixed. Therefore moment reactions do not work, which greatly simplifies the expression of the external work W (see equation 5.32).
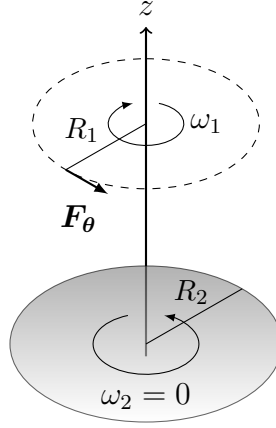
Figure 5-9: Problem statement of Michell cantilever.

5.3.2 Volume of 3D Michell cantilever

Adapting section 5.2.5 *Volume of Michell sphere* to the cantilever loading condition described in section 5.3.1, the work of external forces W is here:

$$W = F_\theta R_1 \omega_1 \tag{5.32}$$

The disc of radius R_2 being a support, its work is zero-valued, and $\omega_2 = 0$.

Applying equations 5.32 and 5.15 in equation 3.1, we can compute the minimal volume V_m of the 3D Michell cantilever:

$$V_m = \frac{2}{\sigma} F_\theta R_1 \left[\ln\left(\tan\left(\frac{\varphi_2}{2}\right)\right) - \ln\left(\tan\left(\frac{\varphi_1}{2}\right)\right) \right] \tag{5.33}$$

We have reordered indices 1 and 2 in the above equation for the result to be positive. Let's note the mix of similarity and singularity this equation has with respect to equation 4.20, giving the volume of the two dimensional Michell cantilever.

5.3.3   Generation of solutions

Depending on the respective values of R_1 and R_2, the substructures have different shapes - even though they have the same line layout as in equation 5.21. The reason is that initial and final torque radii R_1 and R_2 dictate what piece of equation 5.21 shall be analyzed.

Figure 5-10 shows how the cantilever shape changes the discs radii. Figure 5-11 shows more views of the typical solutions.
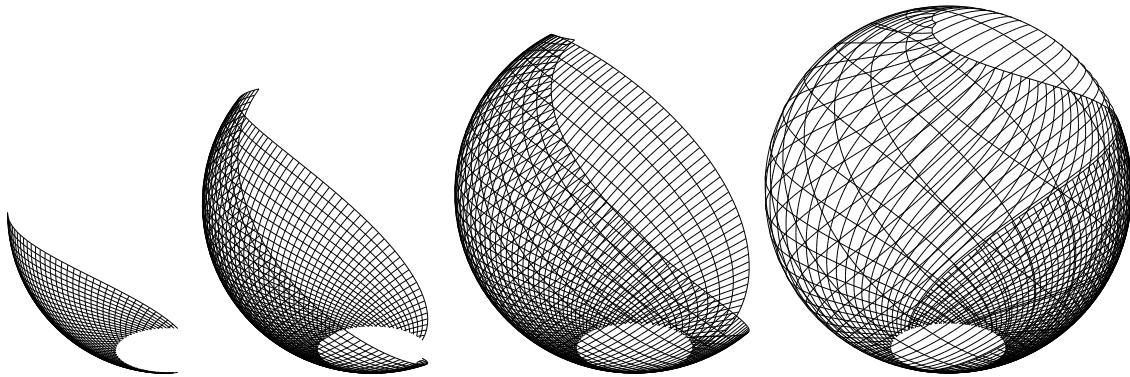
Figure 5-10: Evolution of the cantilever solution: $R_1 = 3R_2$, $2R_2$, R_2 and $\frac{R_2}{5}$.

(a) Case $R_1 > R_2$.

(b) Case $R_1 < R_2$.
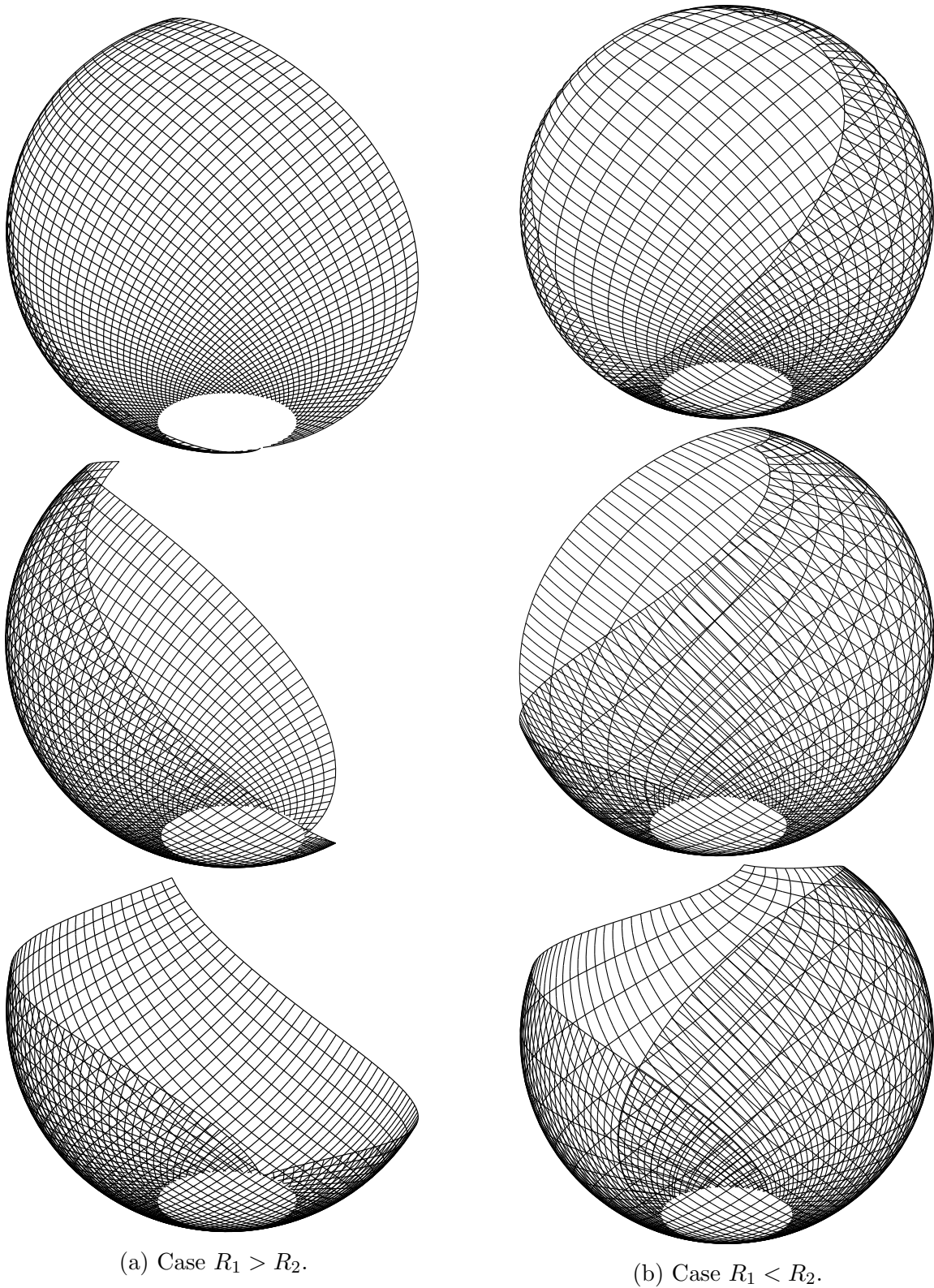
Figure 5-11: Views of typical 3D Michell cantilever solutions.

5.4 Case study: Spinning spheres

5.4.1 Problem statement

We now define a different load case, which, to date, has not been studied. We consider two concentric spheres, called spinning spheres, S_1 and S_2 with different radii R_1 and R_2, such that $R_1 < R_2$. Their common center is O and they are the boundaries of the 3D design domain Ω under consideration.

The angular displacements ω_1 and ω_2 on each sphere are constant. Therefore, each sphere rotates in an uniform way. Then, because both the geometry and the motion conditions of the problem are invariant with respects to θ, θ will not be a variable for any function describing the problem.
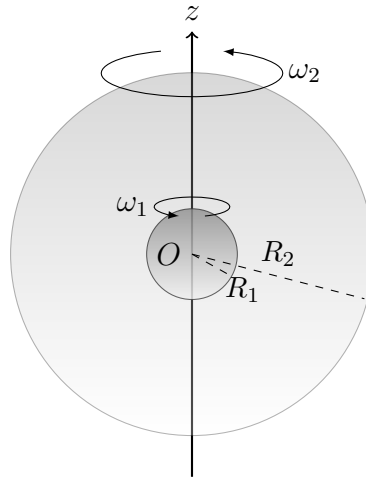
Figure 5-12: Scheme and notations for the spinning spheres problem.

The angular displacement $\omega(r)$ within Ω is unknown at the moment. It is not a function of φ so as to perpetuate the uniform rotation that S_1 and S_2 experience. Yet, it has to satisfy the boundary conditions:

$$\begin{cases} \omega(R_1) = \omega_1 \\ \omega(R_2) = \omega_2 \end{cases} \tag{5.34}$$

A displacement is equal to the angular displacement times its distance to the rotation

axis - here the z axis. We therefore have:

$$\boldsymbol{u}(r, \varphi) = r \sin(\varphi) \omega(r) \boldsymbol{e_\theta} \tag{5.35}$$

5.4.2 Finding the strain tensor

We use equation 5.35 in equation 3.1 and find, per Sadd[24], chapter 2, equation (2.7.5):

$$\boldsymbol{\varepsilon} = \frac{1}{2} \left(\boldsymbol{\nabla u} + \boldsymbol{\nabla u}^{\mathsf{T}} \right) = \varepsilon_{r\theta}(r, \varphi) \boldsymbol{M_{r\theta}} \tag{5.36}$$

$\varepsilon_{r\theta}(r, \varphi)$ is such that:

$$\varepsilon_{r\theta}(r, \varphi) = r \frac{\mathrm{d}\omega}{\mathrm{d}r} \frac{\sin(\varphi)}{2} \tag{5.37}$$

Also, $\boldsymbol{M_{r\theta}}$ is defined as:

$$\boldsymbol{M_{r\theta}} = \begin{pmatrix} 0 & 0 & 1 \\ 0 & 0 & 0 \\ 1 & 0 & 0 \end{pmatrix} \tag{5.38}$$

Per equation 5.36, the trace of $\boldsymbol{\varepsilon}$ is equal to zero. Therefore the volumetric strain tensor $\boldsymbol{\varepsilon_{vol}} = \frac{1}{3} tr(\boldsymbol{\varepsilon}) \boldsymbol{I}$ is zero valued. The strain field is hence a shear-only field, as the deviatoric strain tensor $\boldsymbol{\varepsilon_{dev}} = \boldsymbol{\varepsilon} - \boldsymbol{\varepsilon_{vol}}$ is not zero-valued.

In either 2D or 3D, shear is actually what makes Michell structures curved and complex. Indeed, a no-shear case is such that $\boldsymbol{\varepsilon} = \boldsymbol{\varepsilon_{vol}}$. $\boldsymbol{\varepsilon}$ is therefore a diagonal matrix and its eigenvectors are those of its basis vectors. As a result, steps relating to diagonalizing the strain tensor in MSTM can be skipped. The resulting Michell structure will be a regular and rather simple grid.

A more physical explanation of the above discussion is that no rotation of an elementary section or volume is needed if the latter is submitted to compressive or tensile forces only. Shear is indeed what makes an elementary section or volume rotate in order to find its principal strains.

Returning to the case study, let's see if the way we have defined $\boldsymbol{u}(r, \varphi)$ in equation 5.35 leads to a solution. Based on equation 5.36, maximal and minimal eigenvalues

of the strain tensor ε_I and ε_III are:

$$\begin{cases} \varepsilon_\mathrm{I} = \varepsilon_{r\theta}(r, \varphi) \\ \varepsilon_\mathrm{III} = -\varepsilon_\mathrm{I} \end{cases} \tag{5.39}$$

Applying Lewinsky's criteria, we shall verify $\varepsilon_\mathrm{I} = \varepsilon$, with ε a constant parameter. This brings:

$$r\frac{\mathrm{d}\omega}{\mathrm{d}r}\sin(\varphi) = 2\varepsilon \tag{5.40}$$

The left-hand side of equation 5.40 is a product of a function of r, $r\frac{\mathrm{d}\omega}{\mathrm{d}r}$, by a function of φ, $\sin(\varphi)$. This product has to be equal to the constant in the right-hand side of the equation, 2ε. Therefore both (1) $r\frac{\mathrm{d}\omega}{\mathrm{d}r}$ and (2) $\sin(\varphi)$ shall be constant.

Let's first consider (2). It implies that if a Michell structure exists, it will necessarily have every members lying on two cones of equation $\varphi = \varphi_0$ and $\varphi = \pi - \varphi_0$, with $\varphi_0 \in \left]0, \frac{\pi}{2}\right]$, such that $\sin(\varphi)$ is a constant. A typical solution for the spinning spheres problem will therefore be a Michell cone.

With that in mind, let's solve condition (1) - which is equivalent to solving equation 5.40 adapted to condition (2):

$$r\frac{\mathrm{d}\omega}{\mathrm{d}r} = \frac{2\varepsilon}{\sin(\varphi_0)} \tag{5.41}$$

The solution that meets the first boundary condition in 5.34 is:

$$\omega(r) = \frac{2\varepsilon}{\sin(\varphi_0)}\ln\left(\frac{r}{R_1}\right) + \omega_1 \tag{5.42}$$

The second boundary condition from equation 5.34 is met if:

$$\varepsilon = \sin(\varphi_0)\frac{\omega_2 - \omega_1}{2}\left(\ln\left(\frac{R_2}{R_1}\right)\right)^{-1} \tag{5.43}$$

Hence:

$$\omega(r) = (\omega_2 - \omega_1)\frac{\ln\left(\dfrac{r}{R_1}\right)}{\ln\left(\dfrac{R_2}{R_1}\right)} + \omega_1 \tag{5.44}$$

Hence, there are solutions that meet both Lewinsky's criteria (equation 5.40) and the

boundary conditions (equations 5.42 and 5.43). They define a family of Michell structures for the problem, parametrized by φ_0. If all structures have constant maximal and minimal principal strains, which are equal in absolute value and opposed, they may not all be of minimal volume though.

More precisely, equation 5.43 shows that the principal strains vary with φ_0: $\varepsilon_I = -\varepsilon_{III} = \varepsilon(\varphi_0)$. The volume for each Michell structure, as defined in equation 2.20, will therefore vary with φ_0 as well. Section 5.4.3 *Volume of the Michell cones* will show how the volume of a given Michell structure vary with the parameter φ_0.

In view of what precedes, displacement $\boldsymbol{u}$ and strain tensor $\boldsymbol{\varepsilon}$ are:

$$\boldsymbol{u} = r \sin(\varphi_0) \left((\omega_2 - \omega_1) \frac{\ln\left(\dfrac{r}{R_1}\right)}{\ln\left(\dfrac{R_2}{R_1}\right)} + \omega_1 \right) \boldsymbol{e_\theta} \tag{5.45}$$

$$\boldsymbol{\varepsilon} = \sin(\varphi_0) \frac{\omega_2 - \omega_1}{2} \left(\ln\left(\frac{R_2}{R_1}\right) \right)^{-1} \boldsymbol{M_{r\theta}} \tag{5.46}$$

5.4.3 Volume of the Michell cones

For a moment or torque T applied on $R = R_2$, external equilibrium brings that the torque applied on $R = R_1$ is $-T$. The work of external forces is:

$$W = T(\omega_2 - \omega_1) \tag{5.47}$$

Combining this equation with equations 2.20 and 5.43, the volume of the Michell structure is:

$$V_m = \frac{2T}{\sigma \sin(\varphi_0)} \ln\left(\frac{R_2}{R_1}\right) \tag{5.48}$$

The absolute minimal structure is found for $\varphi_0 = \frac{\pi}{2}$, which corresponds to the 2D Michell wheel - as shown in section 4.1 *Case study: Michell wheel*. Interestingly enough, this two-dimensional Michell structure is the optimal solution for the three-dimensional case under consideration - which would have been challenging to intuit.

Defining the performance score $\gamma(\varphi_0)$ as the economical performance of the Michell structure located on cones $\varphi = \varphi_0$ and $\varphi = \pi - \varphi_0$, we find:

$$\gamma(\varphi_0) = \frac{V_m(\varphi_0)}{V_m(\pi/2)} = \frac{1}{\sin(\varphi_0)} \tag{5.49}$$

Let's emphasize that the Michell structure on cones $\varphi = \varphi_0$ and $\varphi = \pi - \varphi_0$ may not be the optimal solution within Ω, but it becomes the optimal solution within $\Omega \cap D$, where D is the region of space in which φ is such that $|\pi/2 - \varphi_0| \leq |\pi/2 - \varphi|$.

5.4.4 Parametric generations based on the tensor method

Figure 5-13 shows the family of Michell structures solution of the problem, parametrized by their colatitude φ_0. The figure also displays the corresponding volume-based performance scores $\gamma(\varphi_0)$ for each solution.

5.4.5 Equation of the Michell cones lines

From equation 5.46, eigenvectors $\boldsymbol{\pi}_{\mathrm{I}}$ and $\boldsymbol{\pi}_{\mathrm{III}}$ of $\boldsymbol{\varepsilon}$ corresponding to the maximal eigenvalue ε_I and minimal one $\varepsilon_{\mathrm{III}}$ respectively are such that:

$$\begin{cases} \boldsymbol{\pi}_{\mathrm{I}} \parallel \boldsymbol{e_r} + \boldsymbol{e_\theta} \\ \boldsymbol{\pi}_{\mathrm{III}} \parallel \boldsymbol{e_r} - \boldsymbol{e_\theta} \end{cases} \tag{5.50}$$

Re-using equation 5.17, we want to verify that $\mathrm{d}\boldsymbol{OM} \parallel \boldsymbol{\pi}_{\mathrm{I}}$ *or* $\boldsymbol{\pi}_{\mathrm{III}}$. Per equation 5.50, we find:

$$\begin{cases} r\,\mathrm{d}\varphi = 0 \\ \mathrm{d}r = \pm r\sin(\varphi)\,\mathrm{d}\theta \end{cases} \tag{5.51}$$

As $0 < R_1 \leq r \leq R_2$, we find $\mathrm{d}\varphi = 0$. It shows that the lines of the structure stay on a same conical surface, which equation is $\varphi = \varphi_0$. Using the second equation in 5.51, let's solve:

$$\frac{\mathrm{d}r}{\mathrm{d}\theta} \pm \sin(\varphi_0)r = 0 \tag{5.52}$$

$\gamma\left(\dfrac{\pi}{10}\right) = 3.24$

$\gamma\left(\dfrac{\pi}{5}\right) = 1.70$

$\gamma\left(\dfrac{3\pi}{10}\right) = 1.24$

$\gamma\left(\dfrac{2\pi}{5}\right) = 1.05$

$\gamma\left(\dfrac{\pi}{2}\right) = 1$
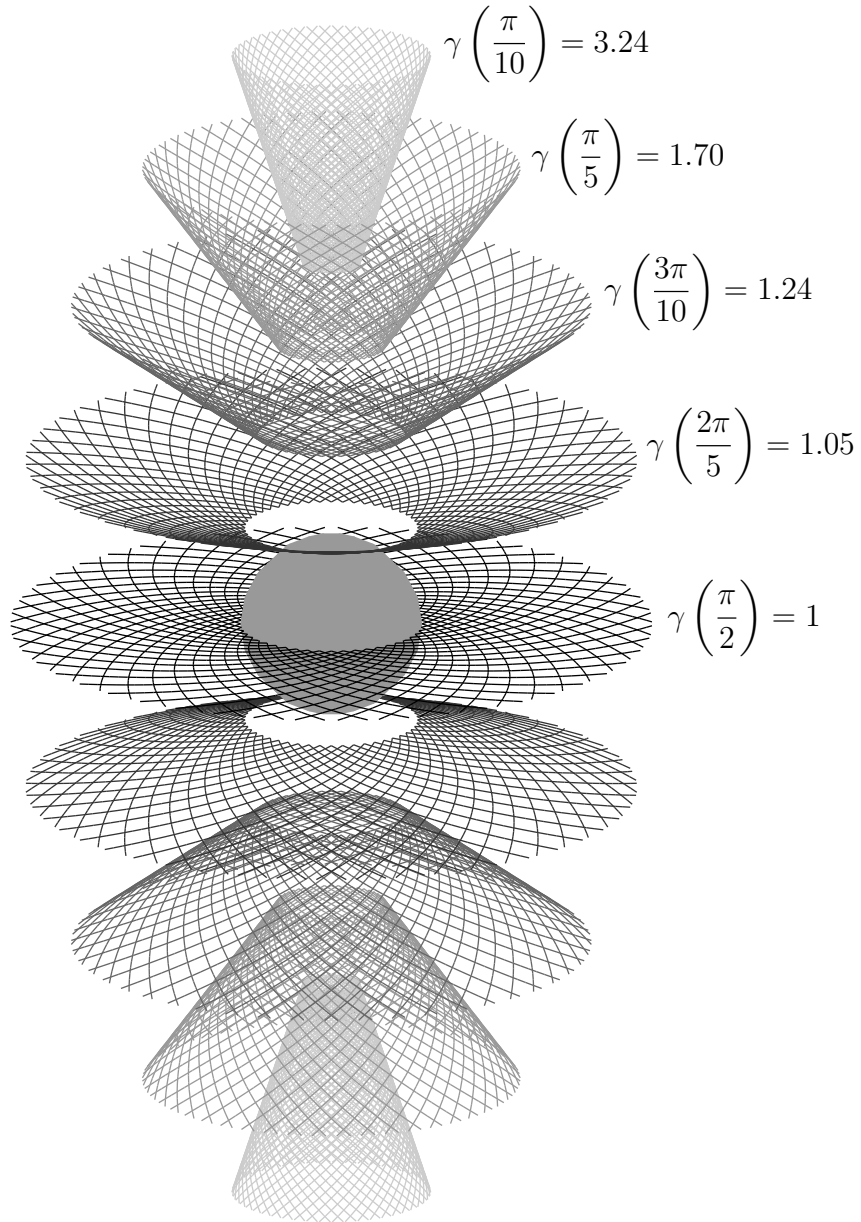
Figure 5-13: Different Michell structures. The darker the structure, the more economically efficient.

The solution of the above differential equation is:

$$r(\theta) = R_1 e^{\pm \sin(\varphi_0)(\theta - \theta_0)} \tag{5.53}$$

We added the condition $r(\theta = \theta_0) = R_1$ to find the above function. By varying φ_0 and θ_0, we plot the lines defined in equation 5.53 in figure 5-14.
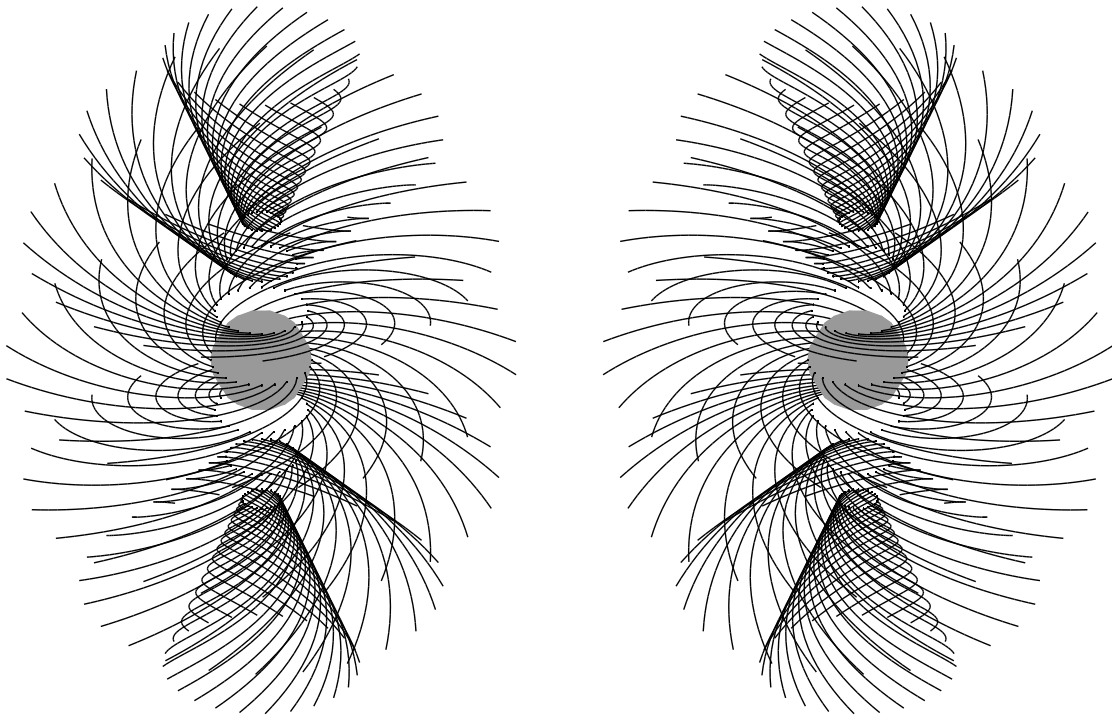
Figure 5-14: The two sets of lines from equation 5.53 - compression or tension.

Chapter 6

Conclusions

This chapter summarizes the work presented in this thesis and explains what the next steps in the field of research about three-dimensional Michell structures should be. It also shows what the potential impact of this research may be.

6.1   Summary of contributions

A new method for finding Michell structures has been defined in order to find solutions for three-dimensional problems: the Michell strain tensor method, or MSTM. the latter has been proved equivalent to the existing mathematical methods, with the advantage of easier application to three-dimensional prolems.

The three dimensional Michell structure solution for the transmission of coaxial circular torques with unequal radii has been found.

The three-dimensional Michell structure solution for the transmission of a point load to a circular support has been found.

A family of three-dimensional Michell structures for the spinning spheres problem has been found and is referred as Michell cones. The solution in $\Omega = \mathbb{R}^3$ is the 2D Michell wheel, and Michell cones of equation $\varphi = \varphi_0$ and $\varphi = \pi - \varphi_0$ are the optimum solution

for the spinning sphere problem within the particular domain of space $\Omega = \mathbb{R}^3 \cap D$ where $D = \{M(r, \varphi, \theta) \in \mathbb{R}^3, |\pi/2 - \varphi_0| \leq |\pi/2 - \varphi|\}$.

Also, the Michell cone of equation $\varphi = \varphi_0$ is the solution in $\Omega = \mathbb{R}^3 \cap D$ for the transmission of coaxial circular torques with unequal radii, where $D = \{M(r, \varphi, \theta) \in \mathbb{R}^3, \varphi_0 \leq \varphi\}$ if $R_1 < R_2$ or $D = \{M(r, \varphi, \theta) \in \mathbb{R}^3, \varphi \leq \varphi_0\}$ if $R_1 > R_2$. It is not as economical as the Michell sphere solution though, because it does not have as much spatial freedom as the latter.

6.2 Future work

This section explains what the next steps in the research about three-dimensional Michell structures should be.

Investigating how the volumes of Michell structures vary when reducing Ω could be an interesting study to perform. The origin of the coordinate system being different between sections 5.2 and 5.4, the corresponding equations for the volume should be compared with extra care in future work.

A study about how to make the complex variables theory work in two-dimensional cases with Michell's rule should be performed, so as to replicate Hemp structures[7], for which maximal allowable tension and compression stresses are not equal. New two-dimensional case studies could hence be solved.

The case studies that are shown in this thesis are analytically solvable, mostly because their geometrical aspect fits well with the coordinate system we used: namely, the polar and spherical coordinate systems. For this reason, other three-dimensional case studies can be investigated relying on the cylindrical coordinate system, and inspiration can be found in Lagache[28].

Complex loading conditions in three dimensions are sometimes difficult to solve analytically: for example, when $R_1 = 0$ in section 5.3 *Case study: 3D Michell cantilever* or when spheres have two different axes of rotation in section 5.4 *Case study: Spinning spheres*. In such cases, computational methods shall be used to determine what

the Michell strain field is, or to approximate it the best way possible. Inspiration can be found in Zegard & Paulino[22].

The equivalent of equation 3.2 in three dimensions may be found by rewriting the proof in section 3.2 *Proof of equivalence between MSTM in 2D and Hemp & Chan procedure* in a generic 3D orthogonal curvilinear coordinate system and by applying Lewinsky's criteria. The hypothesis of small displacements should be kept.

In section 2.3 *The mathematics of Michell structures*, it would be of great interest to investigate how Hemp's optimum criteria from equation 2.22 varies when the structure becomes a moment-frame. The expression for the work of internal forces would change but rest of the procedure shown in this section would remain identical. More inspiration can be found in Baker[19], where Lagrangian optimization is performed on the equation of a volume of a structure with the equality in principle of virtual works being a constraint.

6.3 Concluding remarks and potential impact

This thesis defines a new method to find Michell structures: the Michell strain tensor method. The latter paves the way for new three-dimensional Michell structures to be found, hence enabling the transfer of loads from one location in space to another in the most economical way possible. Michell structures have indeed the absolute minimum volume of material required to resist given loading conditions and can be of great interest in several optimization problems in engineering.

Hopefully, such structures will be used in practice as a pattern or as a source of inspiration in the design of economical and beautiful structures in the built environment.

THIS PAGE INTENTIONALLY LEFT BLANK

Chapter 7

Bibliography

[1] Michell A. The limit of economy of material in frame structures. *Phil.Mag. Series VI*, 8, nov 1904.

[2] Vukotic L., Fenner R.A., and Symons K. Assessing embodied energy of building structural elements. *ICE Engineering Sustainability*, Issue ES3:147–158, 2010. doi:`10.1680/ensu.2010.163.3.147`.

[3] De Wolf C. Low-carbon pathways for structural design. Presentation at the Massachusetts Institute of Technology (this is a full UNPUBLISHED entry), October 2015.

[4] Beghini L., Carrion J., Beghini A., Mazurek A., and Baker W. Structural optimization using graphic statics. *Structural and Multidisciplinary Optimization*, 2013. doi:`10.1007/s00158-013-1002-x`.

[5] Mueller C. 2013. StructureFIT design tool, retrieved from www.caitlinmueller.com/structurefit.

[6] Mueller C. and Ochsendorf J. Combining structural performance and designer preferences in evolutionary design space exploration. *Automation in Construction*, 52:70–82, apr 2015. doi:`doi:10.1016/j.autcon.2015.02.011`.

[7] Hemp W. *Optimum structures*, chapter 4, pages 70–101. Oxford engineering science series. Oxford university press, 1973.

[8] Stafford-Smith B. and Coull A. *Tall building structures : Analysis and Design.* John Wiley & Sons, 1991.

[9] Zalewski W. 2005. Michell projects, retrieved from https://stuff.mit.edu/afs/athena/dept/cron/Backup/project/zalewski/projects/michell/.

[10] SOM San Francisco. *Nature and structure: structural efficiency through natural geometries.* Skidmore, Owings and Merrill LLP, dec 2011.

[11] Ghista D. and Resnikoff M. Development of michell minimum weight structures. *NASA Technical Notes*, D-4345, jan 1968.

[12] Maxwell J. On reciprocal figures, frames and diagrams of force. *The scientific papers of James Clerk Maxwell*, 2:161–207, 1872. doi:`http://dx.doi.org/10.1017/CBO9780511710377.014`.

[13] Baker W. Presentation at SOM Chicago (this is a full UNPUBLISHED entry), jan 2016.

[14] Spillers W. *Iterative Structural Design.* Elsevier, 1975.

[15] Lewinsky T. and Sokol T. On basic properties of michell's structures. *Topology optimization in structural and continuum mechanics*, 549:87–128, 2014. doi:`10.1007/978-3-7091-1643-2_6`.

[16] Rozvany G. Some shortcomings in michell's truss theory. *Structural and Multi-disciplinary Optimization*, 12:244–250, dec 1996. doi:`10.1007/BF01197364`.

[17] Rozvany G. Structural topology optimization (sto) - exact analytical solutions: part i. *Topology Optimization in Structural and Continuum Mechanics*, 549:1–14, 2014. doi:`10.1007/978-3-7091-1643-2_1`.

[18] Chan A. The design of michell optimum structures. *Aeronautical research council reports and memoranda*, 3303, dec 1960.

[19] Baker W. Energy-based design of lateral systems. *Structural Engineering International*, pages 99–102, 1992. doi:`10.2749/101686692780615950`.

[20] Jouve F. Structural shape and topology optimization. *Topology Optimization in Structural and Continuum Mechanics*, 549:129–173, 2014. doi:`10.1007/978-3-7091-1643-2_7`.

[21] Mazurek A., Baker W., and Tort C. Geometrical aspects of optimum truss like structures. *Structural and Multidisciplinary Optimization*, 42:231–242, 2010. doi:`10.1007/s00158-010-0559-x`.

[22] Zegard T. and Paulino G. Ground structure based topology optimization for arbitrary 3d domains using matlab. *Structural and Multidisciplinary Optimization*, 52:1161–1184, 2015. doi:`10.1007/s00158-015-1284-2`.

[23] Victoria M., Querin O., and Marti P. Topology design of three-dimensional continuum structures using isosurfaces. *Advances in engineering software*, 2011. doi:`10.1016/j.advengsoft.2011.05.003`.

[24] Sadd M. *Elasticity: theory, applications and numerics*. Elsevier, 2005.

[25] Love A. *A treatise on the mathematical theory of elasticity*. Cambridge university press, second edition, 1906.

[26] Strang G. and Kohn R. Hencky-prandtl nets and constrained michell trusses. *Computer methods in applied mechanics and engineering*, 36:207–222, feb 1983. doi:`10.1016/0045-7825(83)90113-5`.

[27] Lewinsky T. Michell structures formed on surfaces of revolution. *Structural and Multidisciplinary Optimization*, 28:20–30, 2004. doi:`10.1007/s00158-004-0419-7`.

[28] Lagache J.-M. Treillis de volume minimal dans une région donnée. *Journal de Mécanique*, 20(3), 1981. (French).

THIS PAGE INTENTIONALLY LEFT BLANK

Appendix A

Matlab code for Michell wheel

```matlab
clear all;
close all;

% 1—Domain:
r_1=5;                          % Inner radius
r_2=30;                         % Outer radius
step=1;                         % Step in absolute value

% 2—Loads:
p_1=0;                          % Inner point load
p_2=10;                         % outer normal load

% 3—Generation of the Form
hold on

% 3—1 Starting points definition
alpha=pi/9;
Starting_points=[];
for th=alpha:alpha:(2*pi)
    X_node=[r_2*cos(th);r_2*sin(th)];
    Starting_points=[Starting_points,X_node];
end

% 3—2 First Iteration
```

```
l=length(Starting_points(1,:));
Next_Starting_points=[];
for i=1:1:l
    X_0=Starting_points(:,i);
    [M]=HollowTubeMatrix(X_0(1,1),X_0(2,1),p_1,p_2,r_1,r_2);
    [lambda_1,lambda_2,Pi_1,Pi_2]=TwoDimEigen(M);
    if longueur(X_0+step*Pi_1)<longueur(X_0)
        X_1=X_0+step*Pi_1;
    else
        X_1=X_0-step*Pi_1;
    end
    if longueur(X_0+step*Pi_2)<longueur(X_0)
        X_2=X_0+step*Pi_2;
    else
        X_2=X_0-step*Pi_2;
    end
    plot([X_0(1,1) X_1(1,1)],[X_0(2,1) X_1(2,1)],'-k');
    plot([X_0(1,1) X_2(1,1)],[X_0(2,1) X_2(2,1)],'-k');
    Next_Starting_points=[Next_Starting_points,X_1,X_2];
end

% 3-3 Next Iterations
while norm(Next_Starting_points(:,1))>r_1
    Starting_points=Next_Starting_points;
    l=length(Starting_points(1,:));
    Next_Starting_points=[];

    for i=1:1:l
        X_0=Starting_points(:,i);
        [M]=HollowTubeMatrix(X_0(1,1),X_0(2,1),p_1,p_2,r_1,r_2);
        [lambda_1,lambda_2,Pi_1,Pi_2]=TwoDimEigen(M);
        if mod(i,2)==1
            if longueur(X_0+step*Pi_1)<longueur(X_0)
                X_1=X_0+step*Pi_1;
            else
                X_1=X_0-step*Pi_1;
            end
            plot([X_0(1,1) X_1(1,1)],[X_0(2,1) X_1(2,1)],'-k');
            Next_Starting_points=[Next_Starting_points,X_1];
        end
        if mod(i,2)==0
```

```matlab
            if longueur(X_0+step*Pi_2)<longueur(X_0)
                X_2=X_0+step*Pi_2;
            else
                X_2=X_0-step*Pi_2;
            end
            plot([X_0(1,1) X_2(1,1)],[X_0(2,1) X_2(2,1)],'-k');
            Next_Starting_points=[Next_Starting_points,X_2];
        end
    end
end

axis equal; axis off; axis([-1.01*r_2 1.01*r_2,-1.01*r_2 1.01*r_2]);
hold off
%export_fig 'MW_18.eps' '-transparent';
```

THIS PAGE INTENTIONALLY LEFT BLANK

Appendix B

Matlab code for Michell cantilever

```matlab
clear all;
close all;

% 1—Domain:
r_1=3;                          % Inner radius
r_2=30;                         % Outer radius
step=.5;                        % Step in absolute value (shall be lower than
    inner_radius)

% 2—Loads:
p_1=0;                          % Inner point load
p_2=10;                         % outer normal load

% 3—Generation of the Form
hold on

% 3—1 Starting points definition
th=pi;
Starting_points=[r_2*cos(th);r_2*sin(th)];
Next_Starting_points=[];
V=0;

% 3—2 Next Iterations
while norm(Starting_points(:,1))>r_1
```

```
l=length(Starting_points(1,:));
for i=1:1:l
    if i==1||i==l
        X_0=Starting_points(:,i);
        [M]=HollowTubeMatrix(X_0(1,1),X_0(2,1),p_1,p_2,r_1,r_2);
        [lambda_1,lambda_2,Pi_1,Pi_2]=TwoDimEigen(M);
        if longueur(X_0+step*Pi_1)<longueur(X_0)
            X_1=X_0+step*Pi_1;
        else
            X_1=X_0-step*Pi_1;
        end
        if longueur(X_0+step*Pi_2)<longueur(X_0)
            X_2=X_0+step*Pi_2;
        else
            X_2=X_0-step*Pi_2;
        end
        plot([X_0(1,1) X_1(1,1)],[X_0(2,1) X_1(2,1)],'-k');
        plot([X_0(1,1) X_2(1,1)],[X_0(2,1) X_2(2,1)],'-k');
        Next_Starting_points=[Next_Starting_points,X_1,X_2];
        V=V+norm(X_1)+norm(X_2);
    end
    if i<l/2+1 && i>1
        X_0=Starting_points(:,i);
        [M]=HollowTubeMatrix(X_0(1,1),X_0(2,1),p_1,p_2,r_1,r_2);
        [lambda_1,lambda_2,Pi_1,Pi_2]=TwoDimEigen(M);
        if longueur(X_0+step*Pi_2)<longueur(X_0)
            X_2=X_0+step*Pi_2;
        else
            X_2=X_0-step*Pi_2;
        end
        plot([X_0(1,1) X_2(1,1)],[X_0(2,1) X_2(2,1)],'-k');
        Next_Starting_points=[Next_Starting_points,X_2];
    end
    if i>l/2 && i<l
        X_0=Starting_points(:,i);
        [M]=HollowTubeMatrix(X_0(1,1),X_0(2,1),p_1,p_2,r_1,r_2);
        [lambda_1,lambda_2,Pi_1,Pi_2]=TwoDimEigen(M);
        if longueur(X_0+step*Pi_1)<longueur(X_0)
            X_1=X_0+step*Pi_1;
        else
            X_1=X_0-step*Pi_1;
```

```matlab
            end
            plot([X_0(1,1) X_1(1,1)],[X_0(2,1) X_1(2,1)],'-k');
            Next_Starting_points=[Next_Starting_points,X_1];
        end
    end
    Starting_points=Next_Starting_points;
    Next_Starting_points=[];
end
axis equal; axis off; axis([-1.01*r_2 0.2*r_2,-0.5*r_2 0.5*r_2]);
hold off
%export_fig 'MChalf_2D.eps' '-transparent';
```

THIS PAGE INTENTIONALLY LEFT BLANK

Appendix C

Matlab code for Michell sphere

```matlab
clear all;
close all;

%   WARNING: SPHERICAL COORDINATE SYSTEM (R,TH=AZIMUTH,PHI=COLATITUDE)
% 1—Domain:
R=15; r_1=10; r_2=30;      % Radius of sphere, torque 1 and torque 2
step=2;                    % Step in absolute value
alpha=pi/32;               % Radial distribution of starting points on
   Torque 1

% 2—Loads:
M=[0,0,0; ...
   0,0,1; ...
   0,1,0];                 % Strain tensor

% 3—Generation of the Form
C_1=[sqrt(R^2-r_1^2);0;0];     % Position of Torque 1 center
C_2=[sqrt(R^2-r_2^2);0;pi];    % Position of Torque 2 center

hold on

% 3—1 Starting points definition on Torque 1
Starting_points=[];
for a=alpha:alpha:2*pi
```

```matlab
        Node=[R;a;acos(C_1(1,1)/R)];
        Starting_points=[Starting_points,Node];
end

% 3-2 First Iteration
[Pi_M,Pi_m]=TriDimLewinskiEigen(M);   % Defined in the local spherical
    frame
Pi_M=Pi_M'; Pi_m=Pi_m';
l=length(Starting_points(1,:));
Next_Starting_points=[];
for i=1:1:l
    X_0=Starting_points(:,i);
    X_0_M=[X_0(1,1)+step*Pi_M(1,1);...
        X_0(2,1)+step*Pi_M(2,1)/(X_0(1,1)*sin(X_0(3,1)));...
        X_0(3,1)+step*Pi_M(3,1)/X_0(1,1)];
    X_0_m=[X_0(1,1)+step*Pi_m(1,1);...
        X_0(2,1)+step*Pi_m(2,1)/(X_0(1,1)*sin(X_0(3,1)));...
        X_0(3,1)+step*Pi_m(3,1)/X_0(1,1)];
    Next_Starting_points=[Next_Starting_points,X_0_M,X_0_m];
    [X_0(1,1),X_0(2,1),X_0(3,1)]=sph2cart(X_0(2,1),pi/2-X_0(3,1),X_0
        (1,1));
    [X_0_M(1,1),X_0_M(2,1),X_0_M(3,1)]=sph2cart(X_0_M(2,1),pi/2-X_0_M
        (3,1),X_0_M(1,1));
    [X_0_m(1,1),X_0_m(2,1),X_0_m(3,1)]=sph2cart(X_0_m(2,1),pi/2-X_0_m
        (3,1),X_0_m(1,1));
    plot3([X_0(1,1) X_0_M(1,1)],[X_0(2,1) X_0_M(2,1)],[X_0(3,1) X_0_M
        (3,1)],'-k');
    plot3([X_0(1,1) X_0_m(1,1)],[X_0(2,1) X_0_m(2,1)],[X_0(3,1) X_0_m
        (3,1)],'-k');
end

% 3-3 Next Iterations
while max(Next_Starting_points(3,:))<(pi-acos(C_2(1,1)/R))
    Starting_points=Next_Starting_points;
    l=length(Starting_points(1,:));
    Next_Starting_points=[];
    for i=1:1:l
        X_0=Starting_points(:,i);
        if mod(i,2)==1
            X_0_M=[X_0(1,1)+step*Pi_M(1,1);...
            X_0(2,1)+step*Pi_M(2,1)/(X_0(1,1)*sin(X_0(3,1)));...
```

```
                    X_0(3,1)+step*Pi_M(3,1)/X_0(1,1)];
                    Next_Starting_points=[Next_Starting_points,X_0_M];
                    [X_0(1,1),X_0(2,1),X_0(3,1)]=sph2cart(X_0(2,1),pi/2−X_0(3,1)
                        ,X_0(1,1));
                    [X_0_M(1,1),X_0_M(2,1),X_0_M(3,1)]=sph2cart(X_0_M(2,1),pi/2−
                        X_0_M(3,1),X_0_M(1,1));
                    plot3([X_0(1,1) X_0_M(1,1)],[X_0(2,1) X_0_M(2,1)],[X_0(3,1)
                        X_0_M(3,1)],'−k');
                end
                if mod(i,2)==0
                    X_0_m=[X_0(1,1)+step*Pi_m(1,1);...
                    X_0(2,1)+step*Pi_m(2,1)/(X_0(1,1)*sin(X_0(3,1)));...
                    X_0(3,1)+step*Pi_m(3,1)/X_0(1,1)];
                    Next_Starting_points=[Next_Starting_points,X_0_m];
                    [X_0(1,1),X_0(2,1),X_0(3,1)]=sph2cart(X_0(2,1),pi/2−X_0(3,1)
                        ,X_0(1,1));
                    [X_0_m(1,1),X_0_m(2,1),X_0_m(3,1)]=sph2cart(X_0_m(2,1),pi/2−
                        X_0_m(3,1),X_0_m(1,1));
                    plot3([X_0(1,1) X_0_m(1,1)],[X_0(2,1) X_0_m(2,1)],[X_0(3,1)
                        X_0_m(3,1)],'−k');
                end
            end
    end
end
axis equal; axis off; axis([−1.01*R 1.01*R,−1.01*R 1.01*R,−1.01*R 1.01*R
    ]);
view(45,55);
hold off
%export_fig 'MS_10_30_15.eps' '−transparent';
```

THIS PAGE INTENTIONALLY LEFT BLANK

Appendix D

Matlab code for 3D Michell cantilever

```matlab
clear all;
close all;

%    WARNING: SPHERICAL COORDINATE SYSTEM (R,TH=AZIMUTH,PHI=COLATITUDE)
% 1-Domain:
R=30; r_1=15; r_2=10;        % Radius of sphere, torque 1 and torque 2
step=1.5;                     % Step in absolute value
alpha=2*pi;                  % Radial distribution of starting points on
    Torque 1

% 2-Loads:
M=[0,0,0;...
   0,0,1;...
   0,1,0];             % Strain tensor

% 3-Generation of the Form
C_1=[sqrt(R^2-r_1^2);0;0];        % Position of Torque 1 center
C_2=[sqrt(R^2-r_2^2);0;pi];       % Position of Torque 2 center
hold on

% 3-1 Starting points definition on Torque 1
```

```matlab
Starting_points=[];
for a=alpha:alpha:2*pi
    Node=[R;a;acos(C_1(1,1)/R)];
    Starting_points=[Starting_points,Node];
end

% 3-2 Iterations
[Pi_M,Pi_m]=TriDimLewinskiEigen(M);   %Defined in the local spherical
    frame
Pi_M=Pi_M';Pi_m=Pi_m';
l=length(Starting_points(1,:));
Next_Starting_points=[];
while max(Starting_points(3,:))<(pi-acos(C_2(1,1)/R))
    l=length(Starting_points(1,:));
    for i=1:1:l
        if i==1||i==l
            X_0=Starting_points(:,i);
            X_0_M=[X_0(1,1)+step*Pi_M(1,1);...
                X_0(2,1)+step*Pi_M(2,1)/(X_0(1,1)*sin(X_0(3,1)));...
                X_0(3,1)+step*Pi_M(3,1)/X_0(1,1)];
            X_0_m=[X_0(1,1)+step*Pi_m(1,1);...
                X_0(2,1)+step*Pi_m(2,1)/(X_0(1,1)*sin(X_0(3,1)));...
                X_0(3,1)+step*Pi_m(3,1)/X_0(1,1)];
            Next_Starting_points=[Next_Starting_points,X_0_M,X_0_m];
            [X_0(1,1),X_0(2,1),X_0(3,1)]=sph2cart(X_0(2,1),pi/2-X_0(3,1)
                ,X_0(1,1));
            [X_0_M(1,1),X_0_M(2,1),X_0_M(3,1)]=sph2cart(X_0_M(2,1),pi/2-
                X_0_M(3,1),X_0_M(1,1));
            [X_0_m(1,1),X_0_m(2,1),X_0_m(3,1)]=sph2cart(X_0_m(2,1),pi/2-
                X_0_m(3,1),X_0_m(1,1));
            plot3([X_0(1,1) X_0_M(1,1)],[X_0(2,1) X_0_M(2,1)],[X_0(3,1)
                X_0_M(3,1)],'-k');
            plot3([X_0(1,1) X_0_m(1,1)],[X_0(2,1) X_0_m(2,1)],[X_0(3,1)
                X_0_m(3,1)],'-k');
        end
        if i>l/2 && i<l
            X_0=Starting_points(:,i);
            X_0_M=[X_0(1,1)+step*Pi_M(1,1);...
                X_0(2,1)+step*Pi_M(2,1)/(X_0(1,1)*sin(X_0(3,1)));...
                X_0(3,1)+step*Pi_M(3,1)/X_0(1,1)];
            Next_Starting_points=[Next_Starting_points,X_0_M];
```

```matlab
        [X_0(1,1),X_0(2,1),X_0(3,1)]=sph2cart(X_0(2,1),pi/2-X_0(3,1)
            ,X_0(1,1));
        [X_0_M(1,1),X_0_M(2,1),X_0_M(3,1)]=sph2cart(X_0_M(2,1),pi/2-
            X_0_M(3,1),X_0_M(1,1));
        plot3([X_0(1,1) X_0_M(1,1)],[X_0(2,1) X_0_M(2,1)],[X_0(3,1)
            X_0_M(3,1)],'-k');
    end
    if i<l/2+1 && i>1
        X_0=Starting_points(:,i);
        X_0_m=[X_0(1,1)+step*Pi_m(1,1);...
            X_0(2,1)+step*Pi_m(2,1)/(X_0(1,1)*sin(X_0(3,1)));...
            X_0(3,1)+step*Pi_m(3,1)/X_0(1,1)];
        Next_Starting_points=[Next_Starting_points,X_0_m];
        [X_0(1,1),X_0(2,1),X_0(3,1)]=sph2cart(X_0(2,1),pi/2-X_0(3,1)
            ,X_0(1,1));
        [X_0_m(1,1),X_0_m(2,1),X_0_m(3,1)]=sph2cart(X_0_m(2,1),pi/2-
            X_0_m(3,1),X_0_m(1,1));
        plot3([X_0(1,1) X_0_m(1,1)],[X_0(2,1) X_0_m(2,1)],[X_0(3,1)
            X_0_m(3,1)],'-k');
    end
    end
    Starting_points=Next_Starting_points;
    Next_Starting_points=[];
end
axis equal; axis off; axis([-1.01*R 1.01*R,-1.01*R 1.01*R,-1.01*R 1.01*R
    ]);
view(60,25)
hold off
%export_fig 'MCb_60.eps' '-transparent';
```

THIS PAGE INTENTIONALLY LEFT BLANK

Appendix E

Matlab code for spinning spheres

```matlab
clear all;
close all;

%   WARNING: SPHERICAL COORDINATE SYSTEM (R,TH,PHI)
%   (Different from Chapter 5 convention)
% 1—Domain:
r_1=10; r_2=35;        % Bowls 1 & 2 radii
step=1;                % Step in absolute value
th_s=pi/24;            % Radial distribution of starting points on Bowl 1
phi_s=pi/10;           % Azimutal distribution of starting points on Bowl 1
hstep=0;               % For exploded view
w=0.3;                 % Line width
% 2—Loads:
M=[0,1,0; ...
   1,0,0; ...
   0,0,0];             % Strain tensor for this coordinate sys. convention

% 3—Generation of the Form
hold on
for phi=phi_s:phi_s:(pi—phi_s)
    gradient=abs(phi—pi/2)/(pi/2);
    g = gradient*[1 1 1];
    % 3—1 Starting points definition on Bowl 1
    Starting_points=[];
```

113

```matlab
for th=th_s:th_s:2*pi
    Node=[r_1;th;phi];
    Starting_points=[Starting_points,Node];
end

% 3-2 First Iteration
l=length(Starting_points(1,:));
Next_Starting_points=[];
[Pi_M,Pi_m]=TriDimLewinskiEigen(M);
Pi_M=Pi_M'; Pi_m=Pi_m';
if Pi_M(1,1)<0
    Pi_M=-Pi_M;
end
if Pi_m(1,1)<0
    Pi_m=-Pi_m;
end
Z=(1-phi/(pi/2))*hstep;
for i=1:1:l
    X_0=Starting_points(:,i);
    X_0_M=[X_0(1,1)+step*Pi_M(1,1);...
    X_0(2,1)+step*Pi_M(2,1)/(X_0(1,1)*sin(X_0(3,1)));...
    X_0(3,1)+step*Pi_M(3,1)/X_0(1,1)];
    X_0_m=[X_0(1,1)+step*Pi_m(1,1);...
    X_0(2,1)+step*Pi_m(2,1)/(X_0(1,1)*sin(X_0(3,1)));...
    X_0(3,1)+step*Pi_m(3,1)/X_0(1,1)];
    Next_Starting_points=[Next_Starting_points,X_0_M,X_0_m];
    % plot of new iteration
    [X_0(1,1),X_0(2,1),X_0(3,1)]=sph2cart(X_0(2,1),pi/2-X_0(3,1)...
        ,X_0(1,1));
    [X_0_M(1,1),X_0_M(2,1),X_0_M(3,1)]=sph2cart(X_0_M(2,1),...
        pi/2-X_0_M(3,1),X_0_M(1,1));
    [X_0_m(1,1),X_0_m(2,1),X_0_m(3,1)]=sph2cart(X_0_m(2,1),...
        pi/2-X_0_m(3,1),X_0_m(1,1));
    X_0(3,1)=X_0(3,1)+Z;
    X_0_M(3,1)=X_0_M(3,1)+Z;
    X_0_m(3,1)=X_0_m(3,1)+Z;
    plot3([X_0(1,1) X_0_M(1,1)],[X_0(2,1) X_0_M(2,1)],[X_0(3,1)...
        X_0_M(3,1)],'-k','LineWidth',w,'Color',g);
    plot3([X_0(1,1) X_0_m(1,1)],[X_0(2,1) X_0_m(2,1)],[X_0(3,1)...
        X_0_m(3,1)],'-k','LineWidth',w,'Color',g);
end
```

```matlab
% 3-3 Next Iterations
while max(Next_Starting_points(1,:))<r_2
    Starting_points=Next_Starting_points;
    l=length(Starting_points(1,:));
    Next_Starting_points=[];
    for i=1:1:l
        X_0=Starting_points(:,i);
        if mod(i,2)==1
            X_0_M=[X_0(1,1)+step*Pi_M(1,1);...
            X_0(2,1)+step*Pi_M(2,1)/(X_0(1,1)*sin(X_0(3,1)));...
            X_0(3,1)+step*Pi_M(3,1)/X_0(1,1)];
            Next_Starting_points=[Next_Starting_points,X_0_M];
            Eigenvec_s(:,i)=Pi_M;
            % plot of new iteration
            [X_0(1,1),X_0(2,1),X_0(3,1)]=sph2cart(X_0(2,1),...
                pi/2-X_0(3,1),X_0(1,1));
            [X_0_M(1,1),X_0_M(2,1),X_0_M(3,1)]=sph2cart(X_0_M(2,1)
                ,...
                pi/2-X_0_M(3,1),X_0_M(1,1));
            X_0(3,1)=X_0(3,1)+Z;
            X_0_M(3,1)=X_0_M(3,1)+Z;
            plot3([X_0(1,1) X_0_M(1,1)],[X_0(2,1) X_0_M(2,1)],...
                [X_0(3,1) X_0_M(3,1)],'-k','LineWidth',w,'Color',g);
        end
        if mod(i,2)==0
            X_0_m=[X_0(1,1)+step*Pi_m(1,1);...
            X_0(2,1)+step*Pi_m(2,1)/(X_0(1,1)*sin(X_0(3,1)));...
            X_0(3,1)+step*Pi_m(3,1)/X_0(1,1)];
            Next_Starting_points=[Next_Starting_points,X_0_m];
            Eigenvec_s(:,i)=Pi_m;
            % plot of new iteration
            [X_0(1,1),X_0(2,1),X_0(3,1)]=sph2cart(X_0(2,1),...
                pi/2-X_0(3,1),X_0(1,1));
            [X_0_m(1,1),X_0_m(2,1),X_0_m(3,1)]=...
                sph2cart(X_0_m(2,1),pi/2-X_0_m(3,1),X_0_m(1,1));
            X_0(3,1)=X_0(3,1)+Z;
            X_0_m(3,1)=X_0_m(3,1)+Z;
            plot3([X_0(1,1) X_0_m(1,1)],[X_0(2,1) X_0_m(2,1)],...
                [X_0(3,1) X_0_m(3,1)],'-k','LineWidth',w,'Color',g);
        end
```

```matlab
            end
        end
end
axis equal; axis off;
axis([-1.01*r_2 1.01*r_2,-1.01*r_2 1.01*r_2,...
    -1.01*(r_2+hstep) 1.01*(r_2+hstep)]);
lightGrey = 0.6*[1 1 1]; % It looks better if the lines are lighter
[x,y,z] = sphere(r_1);
surface(.99*r_1.*x,.99*r_1.*y,.99*r_1.*z,...
    'FaceColor',lightGrey,'EdgeColor',lightGrey);
view(0,17.5);
hold off
%export_fig 'MB.eps' '-transparent';
%close all;
```